Available online at www.sciencedirect.com

ScienceDirect

Journal of the Mechanics and Physics of Solids 00 (2016) 1–27

J. Mech. Phys. Solids

The injection of a screw dislocation into a crystal: atomistics vs. continuum elastodynamics

J. Verschueren[1a], B. Gurrutxaga–Lerma[1b], D.S. Balint[b], D. Dini[b], A.P. Sutton[c]

[a]*Department of Materials, Imperial College London, SW7 2AZ London, UK.*
[b]*Department of Mechanical Engineering, Imperial College London, SW7 2AZ London, UK.*
[c]*Department of Physics, Imperial College London, SW7 2AZ London, UK.*

Abstract

The injection (creation) process of a straight screw dislocation is compared atomistically with elastodynamic continuum theory. A method for injecting quiescent screw dislocations into a crystal of tungsten is simulated using non-equilibrium molecular dynamics. The resulting stress fields are compared to the those of elastodynamic solutions for the injection of a quiescent screw dislocation. A number of differences are found: a plane wave emission is observed to emanate from the whole surface of the cut used to create the dislocation, affecting the displacement field along the dislocation line (z), and introducing displacement field components perpendicular to the line (along x and y). It is argued that, in part, this emission is the result of the finite time required to inject the dislocation, whereby the atoms in the cut surface must temporarily be displaced to unstable positions in order to produce the required slip. By modelling this process in the continuum it is shown that the displacements components normal to the dislocation line arise from transient displacements of atoms in the cut surface parallel to x and y. It is shown that once these displacements are included in the elastodynamic continuum formulation the plane wave emission in u_z is correctly captured. A detailed comparison between the atomistic and continuum models is then offered, showing that the main atomistic features can also be captured in the continuum.

Keywords: screw dislocation, edge dislocation, injection, elastodynamics, molecular dynamics

1. Introduction

The creation of dislocations is a key step in the evolution of the plastic response of a material [1]. In many low strain rate applications, the density of dislocations is understood to increase via mechanisms such as Frank-Read sources[2]. At higher strain rates or under intense loading, as in shock loading [3] or nano-indentation [4] respectively, alternative dislocation generation mechanisms such as homogeneous nucleation might come into play [5]. Heterogeneous nucleation of dislocations at crack tips, grain boundaries or second phase particles [6] may also be a significant source of dislocations.

Dynamic Discrete Dislocation Plasticity (D3P) has recently been introduced to model plasticity at very high strain rates through the creation and movement of dislocations using the time-dependent elastic fields of elastodynamics

[1] Both authors contributed equally.

Corresponding author: jonas.verschueren10@imperial.ac.uk

Cut	$y = 0, x > 0$	$x = 0, y > 0$
Boundary condition	$u_z(x,0,t) = \frac{B}{2}\mathrm{H}(x)\mathrm{H}(t)$	$u_z(0,y,t) = \frac{B}{2}\mathrm{H}(y)\mathrm{H}(t)$
$u_z(x,y,t)$	$\frac{B}{2\pi}\arctan\left[\frac{-ty}{-x\sqrt{t^2-b^2r^2}}\right]\mathrm{H}(t-br)$	$\frac{B}{2\pi}\arctan\left[\frac{tx}{-y\sqrt{t^2-b^2r^2}}\right]\mathrm{H}(t-rb)$
$\sigma_{yz}(x,y,t)$	$\frac{\mu B}{2\pi}\frac{tx}{r^2\sqrt{t^2-b^2r^2}}\mathrm{H}(t-br)$	$\frac{\mu B}{2\pi}\frac{tx\left(t^2-b^2\left(x^2+2y^2\right)\right)}{r^2\left(t^2-b^2y^2\right)\sqrt{t^2-b^2r^2}}\mathrm{H}(t-br)$
$\sigma_{xz}(x,y,t)$	$\frac{\mu B}{2\pi}\frac{ty\left(b^2\left(2x^2+y^2\right)-t^2\right)}{r^2\left(t^2-b^2x^2\right)\sqrt{t^2-b^2r^2}}\mathrm{H}(t-br)$	$-\frac{\mu B}{2\pi}\frac{ty}{r^2\sqrt{t^2-b^2r^2}}\mathrm{H}(t-br)$
Mapping	$x \mapsto y, -y \mapsto x$	$x \mapsto -y, y \mapsto x$

Table 1: Elastodynamic field components for a quiescent screw dislocation that is injected at $t = 0$ along $x = 0$ and $y = 0$, for two different positions of the cut surface (either along the positive x or y axes). All the rest of field components are zero by construction[10]. Here μ is the shear modulus, b is the slowness of transverse waves, $B = |\mathbf{B}|$ is the magnitude of the Burgers vector, $r^2 = x^2 + y^2$, σ_{yz} and σ_{xz} are the non-zero stress components, and u_z is the displacement field. The branch cut of $\arctan(a)$ is assumed to be at $\mathrm{Re}[a] < 0$ (i.e., the negative x-axis). Here 'mapping' refers to the coordinate change to pass from the in-column cut convention to the other column's cut convention.

[7, 8]. This paper considers the elastodynamic injection of straight screw (and edge) dislocations. Dislocations are 'injected' into the elastodynamic continuum as dipoles either at designated sources or randomly to simulate homogeneous nucleation. This is the closest one can get in a two dimensional model of dislocation dynamics, such as D3P, to the reality of dislocation nucleation, which always involves the formation of loops or half-loops. The question addressed in this paper is how the injection of a straight dislocation in an elastodynamic continuum maps onto the same process in a crystal with a discrete atomic structure. For this purpose it is simpler to consider a straight screw dislocation involving anti-plane strain. Although the question arose only because D3P is a two-dimensional treatment it is nevertheless surprisingly interesting and revealing about the dynamics of dislocation nucleation in reality.

In an elastic continuum dislocations are usually modelled as Volterra defects involving a surface or 'cut' of vanishing thickness on either side of which the elastic displacement field changes discontinuously by the Burgers vector **B**. When the cut terminates inside the continuum a dislocation exists along the line bounding the cut. In this way the core of a Volterra dislocation has vanishing width because it is a mathematical line, and the elastic fields are singular at the core where they diverge to infinity. The injection of a Volterra dislocation is normally assumed to be instantaneous [9], and modelled using a boundary condition of the type (cf.[10]):

$$u_z(x,0,t) = \frac{B}{2}\mathrm{H}(x)\mathrm{H}(t) \tag{1}$$

where $B = |\mathbf{B}|$ and $H(\cdot)$ is the Heaviside step function. Eqn.1 describes a screw dislocation that is injected at $t = 0$ in position $(x, y) = (0, 0)$, with the dislocation line is along the z-axis; this problem was originally solved by Gurrutxaga-Lerma et al.[10]. This boundary condition specifies that the cut or discontinuity be placed along the positive x-axis; the position of the cut is a priori entirely arbitrary, and other options and conventions may adopted. For instance, table 1 summarises the elastodynamic field components for the case of the cut along the positive x-axis, and that in which the cut is given along the positive y-axis. As can be seen, each case can be recovered from the other by appropriate mapping of the coordinates x and y.

In an atomistic model of injecting a screw dislocation there are at least three significant points of departure from the continuum model that has just been outlined. First, the finite separation of atoms in a crystal ensures that the cut, across which the Burgers displacements of $\mathbf{B}/2$ arise, has a finite thickness. Secondly, as the relative displacement across the cut varies from zero to **B** during the finite time of the injection process, the bonding across the cut is altered significantly and this gives rise to additional stress waves emanating from the cut not described in table 1. Thirdly, the core has a finite width and the elastic fields do not diverge to infinity at the core. As will be seen in the next section, the injection a screw dislocation into a crystal merely by replicating the displacements indicated by eqn.1 is non-trivial.

Section 2 describes the difficulties of using eqn.1 as a method for injecting a screw dislocation in a crystal, and how it has to be modified to make it work when the medium displays translational symmetry. The results for the atomistic injection of a screw dislocation are discussed in section 3. Section 4 revisits the elastodynamic description of the instantaneous injection of a straight screw dislocation, described as a Volterra dislocation. In light of the results presented in section 3, section 5 is devoted to a more detailed study of the way distinct core structures and

non-instantaneous injection processes can be modelled in the continuum, offering analytic solutions for the case of an instantaneously injected ramp-like core screw dislocation, and a gradually injected Volterra screw dislocation; further features observed in the atomistic simulations but not in the continuum are also modelled. Both continuum and atomistic developments are compared in section 6.

By convention, most continuum derivations assume that the cut is along the x-axis (cfr.[11, 1]); in sections 4 and 5 this convention is maintained, and the cut is applied along the positive x-axis. However, the atomistic simulations in section 3 assume the cut is placed along the positive y-axis.

2. Injection of a screw dislocation into a crystal using molecular dynamics

2.1. Crystal structure

Tungsten was selected for this molecular dynamics study because it is almost elastically isotropic, which makes it suitable for comparison with the isotropic elastodynamic theory of [7]. It possesses a body centred cubic (BCC) crystal structure with lattice parameter $d = 3.16$Å. The most common screw dislocation Burgers vector $\mathbf{B}$ is $\frac{1}{2}\langle 111\rangle$ with magnitude B. The core structure of $\frac{1}{2}\langle 111\rangle$ BCC screw dislocations are non-planar and topologically complex [12, 13], but since reproducing the exact core structure is not of interest in this article, this does not hinder the comparison with the continuum results. In order to simulate an infinitely long screw dislocation the z-axis is aligned with the [111] direction in the crystal. fig.1a shows the crystal lattice viewed in projection along this [111] direction. The smallest rectangular repeat cell contains 5 atoms and is defined by the translation vectors

$$\mathbf{t}_1 = \left[\sqrt{2}d, 0, 0\right] = [a, 0, 0] \tag{2}$$

$$\mathbf{t}_2 = \left[0, \sqrt{6}d, 0\right] = [0, b, 0] \tag{3}$$

$$\mathbf{t}_3 = \left[0, 0, \frac{\sqrt{3}d}{2}\right] = [0, 0, c]. \tag{4}$$

$$\tag{5}$$

A cylindrical slab of atoms of thickness $7c$ and radius $R_s = 75d$, with its axis along z, was created, resulting in a BCC lattice containing approximately $214,000$ atoms.

2.2. Molecular dynamics specifications

A Finnis–Sinclair potential for tungsten [14, 15] was used in constant energy MD simulations, initially at 0K. In this study, using a thermostat was decided against in order not to disturb the particles' trajectories and a damping layer controlled the temperature rise following dislocation injection (cf. section 2.2). Time integration was performed using a Velocity Verlet algorithm [16] with a timestep $\Delta t = 0.5$ fs which was deemed to adequately strike the balance between energy conservation and available simulation time.

Periodic boundary conditions were imposed along the cylinder axis to simulate an infinitely long dislocation line. The slab thickness of $7c$ is sufficient to ensure that atoms do not interact with their own periodic images [14]. "Damping boundary conditions" were applied, perpendicular to the cylinder axis in a boundary layer of thickness R_d as shown in fig.1b, to minimise reflections of elastic waves at the cylindrical surface and to mimic a cylinder with infinite radius. Therefore, the physical region for observation of the elastic fields is limited to the central part of the simulated cylinder with boundary effects visible in the boundary layer. The damping is achieved by adding a viscous term $\mathbf{F}_d^{(k)}$ in the Newtonian equation of motion to all atoms k in the outer annulus of the cylinder of thickness R_d:

$$\mathbf{F}_d^{(k)} = -C\left(\frac{r_d}{R_d}\right)^2 \mathbf{v}^{(k)} \tag{6}$$

where r_d is the distance of atom k from the undamped region, C is a positive constant and $\mathbf{v}^{(k)}$ is the velocity of the particle [17]. This functional form ensures a smooth transition between the forces on particles in the undamped and damped regions. In this work $C = 100\text{Nsm}^{-1}$ and $R_d = R_s/4$ where chosen. This value of C was found to maximise the rate of energy dissipation; increasing it further causes reflections at the boundary between the damped and undamped regions.

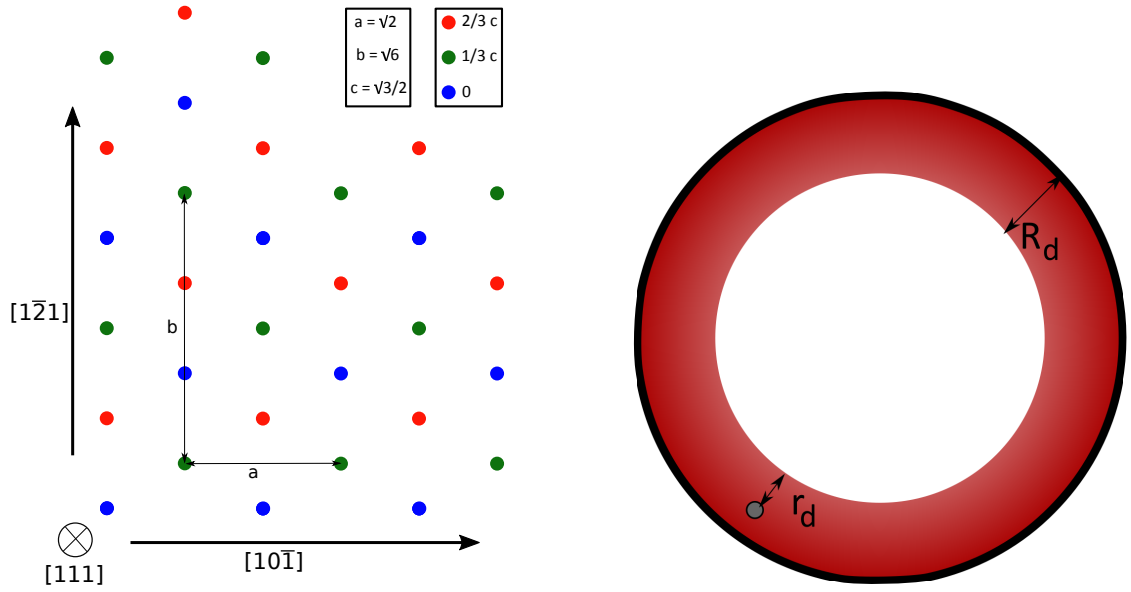

(a) (b)

Figure 1: (a) Atomic structure of BCC crystal viewed in projection along the [111] direction. The three (111) lattice planes in each $d/2$[111] crystal period are coloured red, green and blue. a and b are the lengths of the smallest orthogonal translation vectors $\mathbf{t}_1$ and $\mathbf{t}_2$ parallel to [10$\bar{1}$] and [1$\bar{2}$1] respectively. (b) Cross section of the cylindrical slab used in MD simulations, showing the damped boundary layer of width R_d in red. The distance of an atom in the damped layer to the undamped region is r_d.

This damping boundary condition comes with an additional advantage, as it reduces the need for a computationally expensive surface equilibration. The equilibrated system, in which the screw dislocation is to be injected, has been relaxed using the damping mechanism described above up to a point where the largest force magnitude on any particle in the system is just less than 1.6×10^{-3}eV/ Å. The particles on which the largest forces act are found at the outermost boundary of the cylinder where the damping is strongest and therefore do not interfere with the dynamics of the elastodynamics fields in the undamped central region of the cylinder (cf. fig.1b). Without the damping boundary layer, this would not be sufficiently low to avoid elastic waves propagating in from the boundary. However, including the boundary layer, these unwanted displacement and stress waves are absorbed and their magnitude is insignificant compared to equivalent elastic fields due to the injected dislocation. This was confirmed in trial runs in which a constant energy MD simulation was performed with the equilibrated structure as initial positions and no propagation from the outermost boundary into the central region of the cylinder was seen.

2.3. Dislocation injection into crystals

By the injection of a screw dislocation into a crystal we mean the atomistic equivalent of the continuum boundary condition in eqn.1, and the evolution in time of the subsequent elastic fields, which are the atomistic equivalents of the equations shown in table 1 for the continuum representation. In this section, methods to inject a straight screw dislocation along the axis of an infinitely long crystal cylinder are discussed.

2.3.1. Direct application of equation 1 in a BCC crystal

In the continuum representation of the injection process, eqn.1, a cut is defined on the half-plane $x = 0, y > 0$, and a displacement is introduced along z of $\pm B/2$ at all points on either side of the cut from $y = 0$ to $y = \infty$. All this happens instantaneously at $t = 0$. The only displacements involved at $t = 0$ are therefore confined to planes infinitesimally close to and on either side of the cut: the rest of the continuum has not yet been affected by these displacements. The application of eqn.1 to introduce a $\frac{1}{2}$[111] screw dislocation along the axis of a cylindrical BCC crystal could therefore proceed as follows:

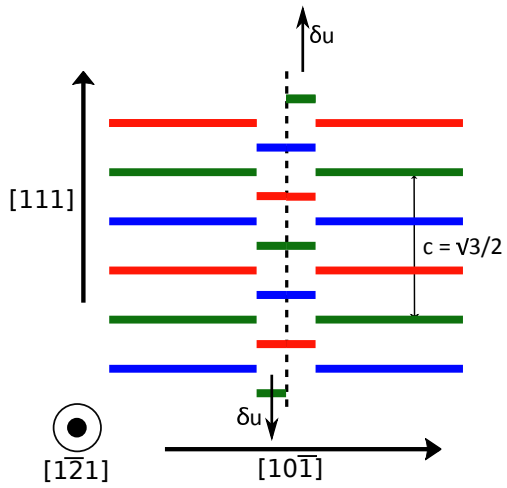

(a) Instantaneous injection

Figure 2: Schematic illustrations of the displacements associated with the instantaneous introduction of a $\frac{1}{2}[111]$ screw dislocation in the region $y > 0$. The crystal is viewed in projection along $[1\bar{2}1]$. The red, green and blue lines are the traces of (111) atomic planes, the colours reflecting the stacking sequence of these planes. The broken black line is the mathematical cut plane passing between two adjacent atomic $(10\bar{1})$ planes. Notice that on the far left and far right the crystals are in perfect registry. There are just two faults caused by the instantaneous injection of a screw dislocation, one on either side of the cut plane. The displacements shown by the arrows have magnitude $\sqrt{3}d/4$.

1. Identify a mathematical plane passing midway between the two adjacent atomic $(10\bar{1})$ planes with the largest area (which defines $x = 0$), extending along $[1\bar{2}1]$ (i.e. along $y > 0$) from the cylinder axis to the surface of the cylinder, and along the entire length of the cylinder.
2. Displace all atoms in the first $(10\bar{1})$ plane on one side of the cut by $\frac{1}{4}[111]$, and all atoms in the first $(10\bar{1})$ plane on the other side of the cut by $-\frac{1}{4}[111]$.
3. Fix the positions of these displaced atoms far from the cylinder axis, and then allow the positions of all other atoms to evolve according to molecular dynamics protocols set out in sections 2.2

The displacements $\pm\frac{1}{4}[111]$ applied to atoms in the adjacent $(10\bar{1})$ half-planes on either side of the cut introduce $(10\bar{1})$ stacking faults in the crystal structure on either side of the cut, where the fault vectors are *both* $\frac{1}{4}[111]$. This is illustrated schematically in Fig. 2. The cut has become a planar defect consisting of a fault extended over four $(10\bar{1})$ half-planes. If a different cut plane normal to [111] is chosen the character of the planar defect also changes. These faults are absent in the continuum.

At $t = 0$ the elastic field of the dislocation has not been created. However the dislocation is nascent because a Burgers circuit enclosing the axis of the cylinder and passing through the two stacking faults will yield the Burgers vector $\mathbf{B} = \frac{1}{2}[111]$. During the subsequent molecular dynamics at $t > 0$ the attempt to eliminate the extended planar defect that the cut has become drives the introduction of the elastic field of the dislocation. At $t = 0$ the total displacement across the cut is everywhere equal to $\mathbf{B}$. But at $t > 0$ this begins to change near the cut plane of the cylinder. Here the crystal begins to accommodate the coexistence in a slab centred on the cut of relative atomic displacements amounting to $\mathbf{B}$ on one side of the axis and no such displacements on the other side. The two stacking faults in fig.2 have to be eliminated far from the dislocation line to return the crystal to an almost perfect state. In principle this is possible because the total fault vector is a lattice translation vector, i.e. $\frac{1}{2}[111]$. In practice it may be very difficult when there are just two faults because the atomic displacements involved are too large. Indeed, this method is found not to yield the elastodynamic fields expected from the equivalent continuum description.

The failure of the direct application of eqn.1 described above can be understood by considering the crystal structure. As shown in fig.2, the instantaneous injection of a screw dislocation in the BCC crystal disrupts the stacking sequence near the cut plane. It was found that this creates a potential barrier for the lattice planes in the immediate vicinity of the cut-plane which impedes the reformation of the perfect lattice on both sides of the cut-plane, removing the stacking fault. This in turn suggests that in a BCC structure, screw dislocations along $\langle 111 \rangle$ type directions

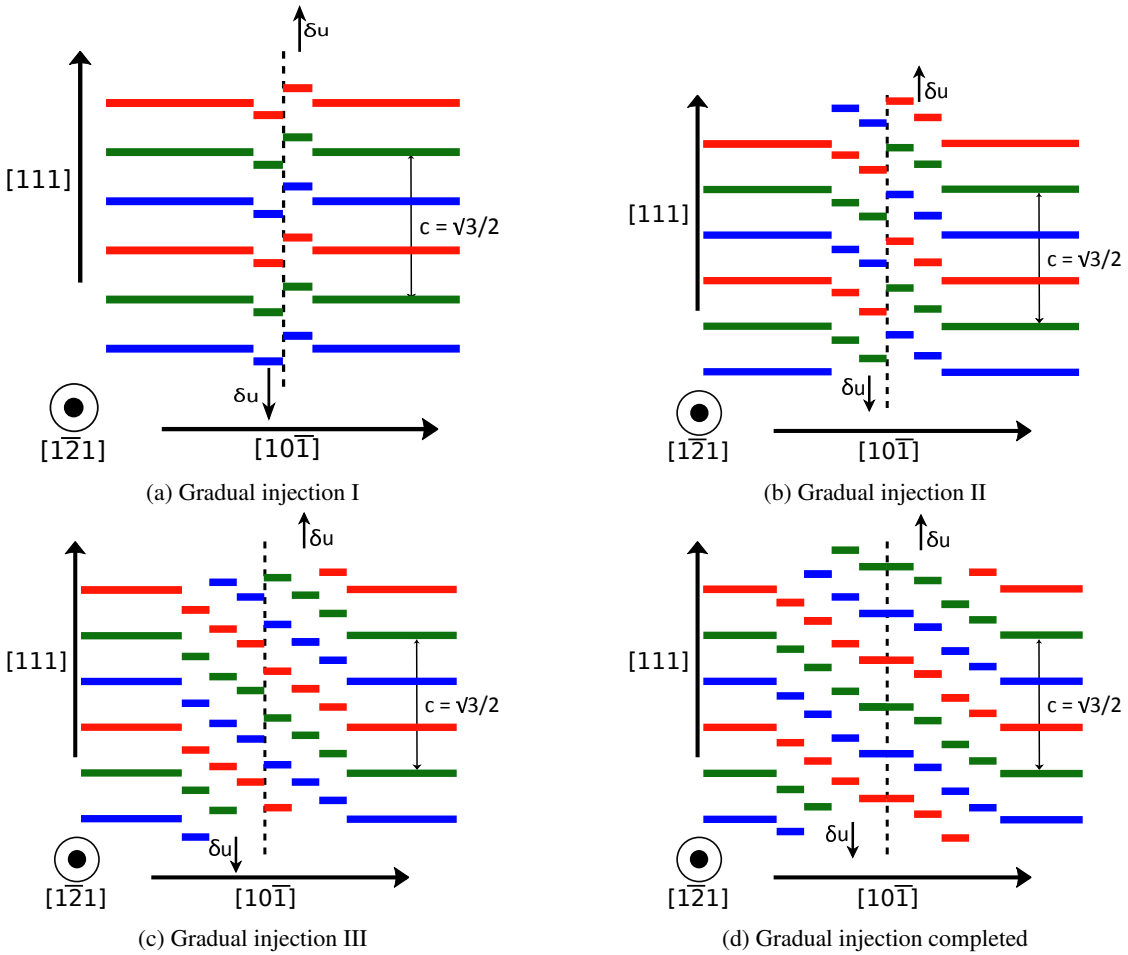

(a) Gradual injection I

(b) Gradual injection II

(c) Gradual injection III

(d) Gradual injection completed

Figure 3: Schematic illustrations of the displacements associated with the gradual introduction of a $\frac{1}{2}[111]$ screw dislocation in the region $y > 0$, analogous to fig.2. In (d) the perfect lattice has reformed across the cut plane but the planes in its vicinity still cause stacking faults. This configuration can be obtained by two equivalent methods. One can build up the displacement jump B across the cut plane as a function of time shown in the time sequence (a), (b), (c) and (d). Alternatively, one can spread the Burgers vector displacement on either side of the cut across a wider region by manually setting up configuration (d) and use this as the initial configuration. It is suggested that although there are more faults in (d) than in fig.2 it is easier to eliminate the faults far from the dislocation line because the atomic displacements required are smaller.

with Burgers vector magnitude c can *only* be achieved in a scheme which preserves the stacking sequence of the lattice planes. This can be achieved in two completely equivalent ways. Firstly, the displacement jump can be built up gradually to a magnitude B over a timespan τ_0, allowing the atoms immediately adjacent to the shifted planes to adjust their positions at every step in the process as shown in the schematic time sequence show in figs.3b, 3c and 3d. Alternatively, the configuration in fig.3d can be set up by spreading the displacement by the Burgers vector on either side of the cut across a wider region L_0. It is clear that both methods are completely equivalent. Whichever is employed, the configuration obtained in fig.3d makes it more likely that the faults will be eliminated far from the dislocation line because the atomic displacements required are smaller in magnitude, though larger in number. The injection parameters L_0 or τ_0 introduce a degree of arbitrariness into the atomistic model that is absent in the continuum. Nevertheless there is a clear physical argument these to be finite in an atomistic model. The gradual injection mechanism was chosen for this work.

Finally, an apparently much simpler procedure to introduce a screw dislocation into the cylindrical crystal is the following. As before, identify the mathematical half-plane passing midway between the two adjacent atomic $(10\bar{1})$ planes with the largest area, extending along $[1\bar{2}1]$ from the cylinder axis to the surface of the cylinder, and along the entire length of the cylinder. This half-plane is designated the cut plane. Displace the first atomic $(10\bar{1})$ plane on one side of this cut by $\frac{1}{2}[111]$. In this case all the displacement associated with the Burgers vector is applied to just one atomic half-plane. However, this method will not generate the screw dislocation owing to the translational symmetry along [111], which is maintained by the use of periodic boundary conditions along this direction. The displacement by all atoms in the $(10\bar{1})$ half-plane by a lattice translation vector parallel to [111] renders the cylindrical crystal invariant! The displacement associated with the Burgers vector has to be distributed over two adjacent $(10\bar{1})$ half-planes to break the translational symmetry along [111] and create the driving force to introduce the elastic field of the dislocation.

The case of an edge dislocation is briefly discussed in Appendix B.

2.3.2. Resolving the instantaneous character of the continuum boundary condition

It is not surprising that the instantaneous character of the injection mechanism proposed in the continuum solution is impossible to reproduce in an atomistic simulation. The aim of formulating the injection of dislocations in an elastodynamic framework was to preserve causality, however this reformulation is built on a boundary condition which by itself is non-local as it requires an *instantaneous* shift of a half-plane of atoms all the way along the entire cut-plane. A ramp function

$$R(t) = \begin{cases} 0 & t < 0 \\ \frac{t}{\tau_0} & 0 \le t \le \tau_0 \\ 1 & t > \tau_0 \end{cases} \tag{7}$$

was chosen to inject a dislocation in a time interval τ_0. This functional form for $R(t)$ proved successful in removing the stacking fault across the cut plane and was used to produce the results presented below, in which the displacement discontinuity was achieved by gradually and simultaneously moving half-planes of atoms up whilst moving half-planes on the other side of the cut-plane down. A temporal ramp width of $\tau_0 = 0.5ps$ was chosen. This value of τ_0 corresponds to an injection velocity of $\sim 10\% c_t$, indicating that elastodynamic effects are expected to be significant. A schematic of this mechanism is shown in figs.3b, 3c and 3d, from which it is obvious that this injection procedure will send an elastic wave through the system. This wave extends all the way along the cut plane, contrary to the elastostatic picture in which perfect lattice positions are assumed away from the dislocation core and stresses are inversely proportional to the distance from the core. This elastostatic configuration will reappear in the elastodynamic formulation as $t \to \infty$.

3. MD results

This section will show that the method proposed above to inject screw dislocations into a crystal works. In addition, the evolution in time of the stress and displacement fields in the atomistic model will be compared with those of the continuum results provided in table 1 for the case of the cut along the positive y-axis.

The ultimate test of whether a screw dislocation has been injected into the crystal is to check that the stress and displacement fields converge after sufficient time to the known static elastic fields [10]. Fig.5 shows this convergence;

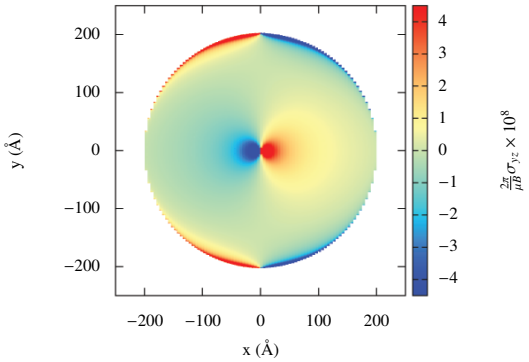

(a) $\sigma_{yz}(x, y, t)$ stress field component, from table 1.

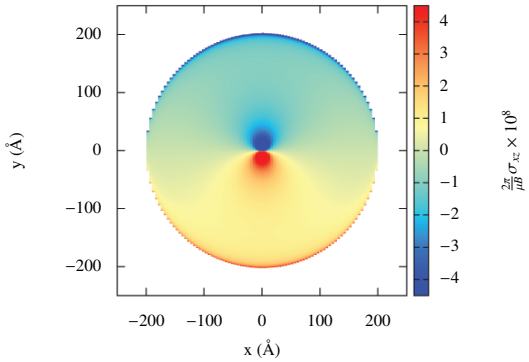

(b) $\sigma_{xz}(x, y, t)$ stress field component, from table 1.

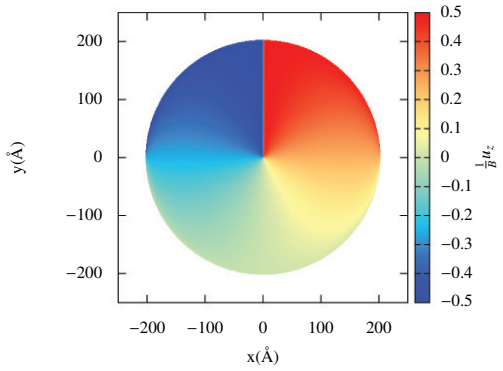

(c) $u_z(x, y, t)$ displacement field component, from table 1.

Figure 4: Elastodynamic stress and displacement fields of an injected, quiescent screw dislocation with the cut along the positive y-axis. Plots for tungsten at t = 7ps, with c_t = 2890m/s. Notice that the system represented here is an infinite, boundless continuum. At 7ps the shear waves have reached 200Å away from the core; the static limit will be reached at $t \to \infty$, at which point the whole space will be occupied by the field of the dislocation.

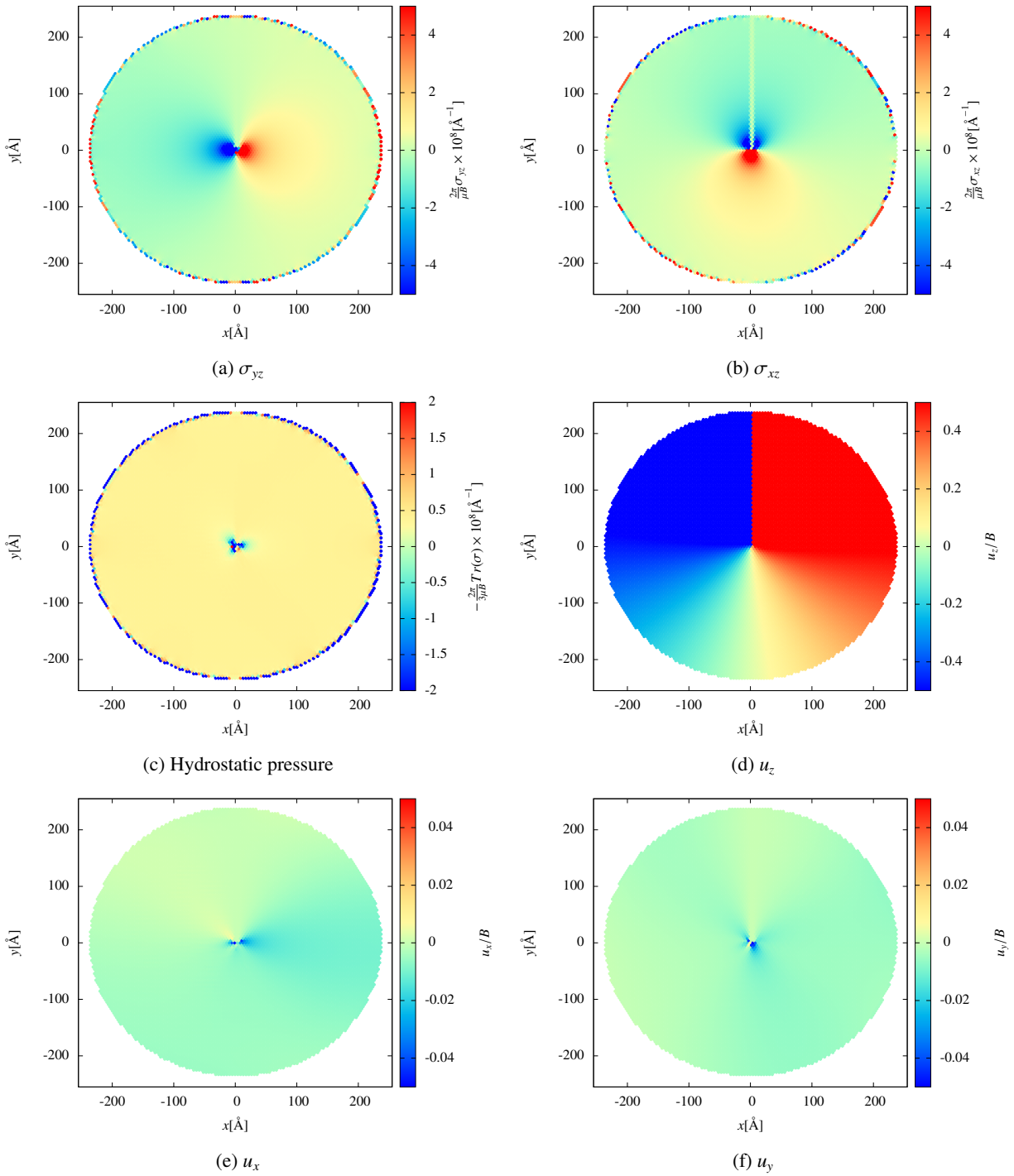

(a) σ_{yz} (b) σ_{xz}

(c) Hydrostatic pressure (d) u_z

(e) u_x (f) u_y

Figure 5: Stress and displacement fields in the MD simulations after $140ps$. Note the qualitative agreement with the corresponding continuum results given in figure 4. The u_x and u_y displacement fields, which are identically zero in the continuum results, vanish in the long-time limit. From (c) it can be seen that the system is under hydrostatic compression attributed to the misfit at the dislocation core.

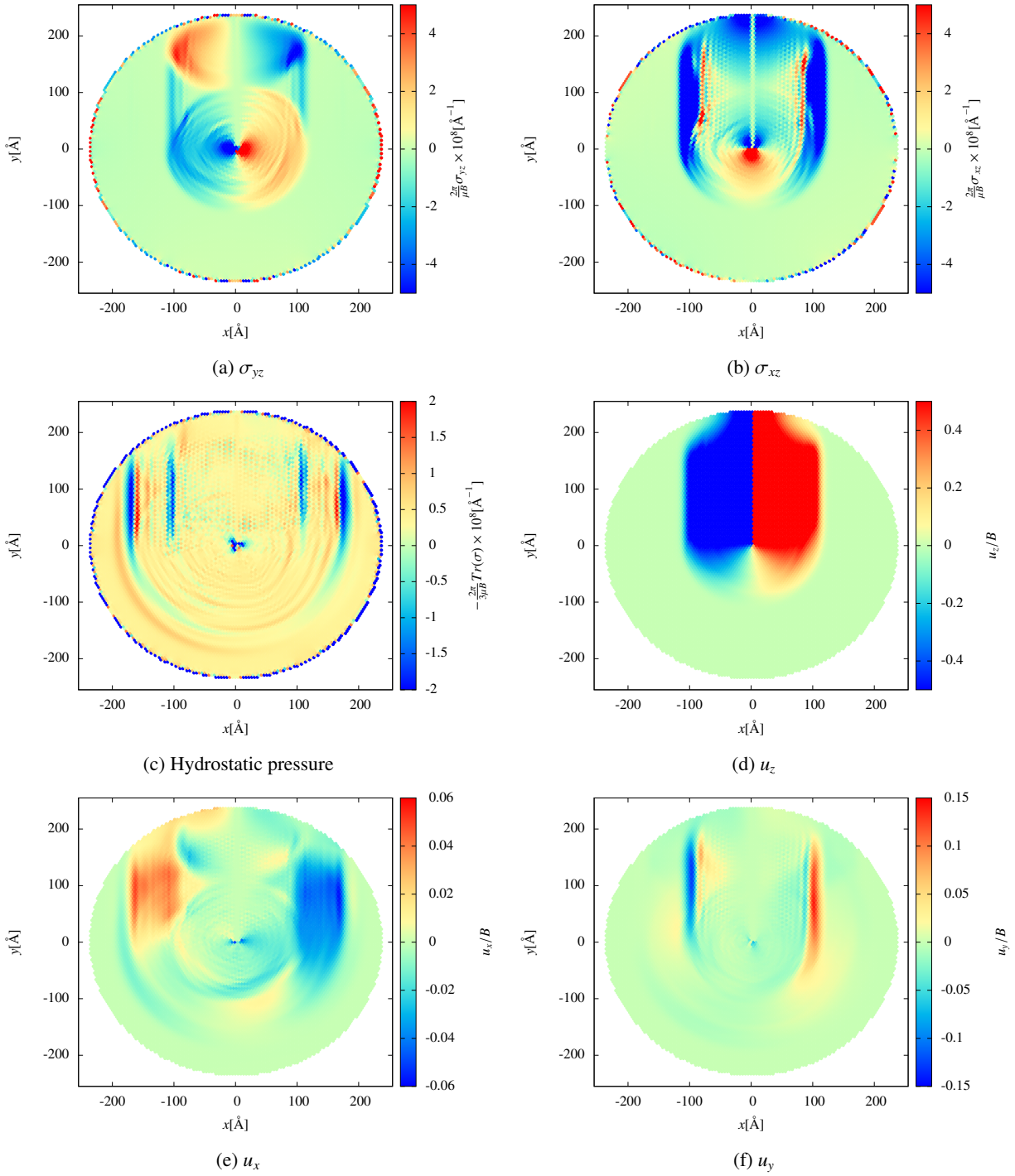

(a) σ_{yz} (b) σ_{xz}

(c) Hydrostatic pressure (d) u_z

(e) u_x (f) u_y

Figure 6: Stress and displacement fields for an injected screw dislocation simulated by molecular dynamics after $3.5ps$ on a cross-sectional (111) lattice plane. The displacement field u_z in (d) shows the displacements spreading from the cut. The stresses introduced by the injection mechanism at the damped/undamped boundary layer are also visible. In (c) and (e) the distinction between the longitudinal and transverse wave fronts can be seen most clearly.

it also indicates that the boundary conditions imposed in the MD simulations were able to simulate a dislocation in an infinite medium in the long time limit.

Transverse wave-fronts are clearly visible in fig.6 also in agreement with the continuum solutions shown in fig.4. These transverse waves travelled at an observed velocity of 2600 ± 300m/s, in reasonable agreement with the experimentally observed value of 2890m/s [18]. Given that the Finnis-Sincair many-body potential used is fitted to the elastic constants of tungsten, which dictate the longitudinal and transverse wave velocities, good agreement is to be expected. Finally, the stress and displacement field magnitudes throughout the whole time sequence from $1 - 140ps$ agree well with their continuum counterparts.

The spreading of the u_z displacement field away from the cut is seen clearly in fig.6d. This feature is missing in the elastodynamic solution given in table 1. This emission was predicted in section 2.3.2, and ascribed to the gradual nature of the injection process, during which the atoms in the vicinity of the cut plane are forced to occupy non-lattice positions. In section 4, it will be shown that albeit hitherto overlooked, the elastodynamic solution for a suddenly injected Volterra dislocation also entails an emission term in u_z, the magnitude of which $(B/2)$ is comparable to the one observed in fig.6d. The elastodynamic emission is described as a planar longitudinal wave front. This is not the case in the molecular dynamics simulations, where the amplitude of the emission is seen to oscillate, most likely due to the gradual injection mechanism and discreteness effects. Despite this, the continuum satisfactorily shows the presence of such transverse emission. Further atomistic effects, such as a weakening of the emission in the environs of the surface, can be attributed to size effects that the continuum description, for dislocations in infinite media, does not account for.

Fig.6 shows transient u_x, u_y and hydrostatic pressure fields. These transients are a result of the initial atomic misfits introduced around the cut. The continuum elastodynamic formulation does not display these transients because the concept of misfit is not applicable to the continuum. The magnitudes of both u_x and u_y components are significantly less than the Burgers vector, suggesting that the misfit components parallel to x and y around the cut are relatively small. This limits the magnitude of the normal stress components associated, so that the elastodynamic fields are eventually dominated by u_z. The atomistic simulations therefore reveal a new feature of the injection of a screw dislocation, namely that the transient displacements fields are three-dimensional, as opposed to their one-dimensional character in the continuum formulation.

Further evidence that the displacement and stress fields in the atomistic simulation that are absent in the elastodynamic continuum solutions are not the product of displacements in u_z can be found in fig.6e, where the emission in u_x is seen to propagate at the longitudinal speed of sound, which does not feature in the elastodynamic description of a screw dislocation whatsoever [10]. The radii of the the longitudinal and transverse wavefronts are estimated from fig.6 to be $\sim$ 74Å and $\sim$ 34Å at 3.5ps. The ratio between the widths of these two emission bands approximately matches the ratio between the observed longitudinal and transverse speeds of sound (5700m/s and 2600m/s respectively).

4. Revisiting the injection of a screw dislocation in an elastodynamic continuum

In light of the MD results, the continuum field solutions derived in [10] are revisited in this section. But first, the standard elastodynamic derivation is reviewed [10]. The governing equation of the elastodynamic continuum is the Navier-Lamé equation, built on the principle of conservation of linear momentum; it is given by [19]

$$(\Lambda + \mu)u_{j,ij} + \mu u_{i,jj} = \rho u_{i,tt} \tag{8}$$

where Λ and μ are Lamé 's first and second constants, and ρ is the material density. The comma denotes differentiation, the subscript t denotes time, u_i is the displacement field, and Einstein's summation convention is assumed except $u_{i,tt} = \partial^2 u_i/\partial t^2$. This equation must be combined with appropriate boundary conditions to describe the injection process.

Consider the Cartesian basis shown in fig.7; the infinitely long screw dislocation is parallel to the z-axis. The only component of the displacement vector that is not zero is u_z. Therefore eqn.8 reduces to

$$u_{z,xx} + u_{z,yy} = b^2 u_{z,tt} \tag{9}$$

where $1/b = c_t = \sqrt{\mu/\rho}$ is the transverse speed of sound in the material—and b the corresponding transverse slowness of sound.

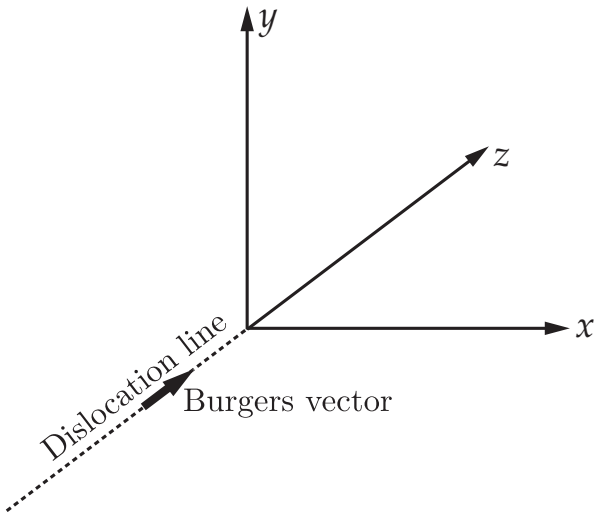

Figure 7: Coordinate system for the continuum modelling of the infinite straight screw dislocation.

The introduction of the necessary displacement jump at time of injection $t = 0$ is achieved by imposing the boundary condition

$$u_z(x, 0, t) = \frac{B}{2}\mathrm{H}(x)\mathrm{H}(t) \tag{10}$$

where B is the magnitude of the Burgers vector and $\mathrm{H}(\cdot)$ is the Heaviside step function. It must be noted that this prescribes a cut surface along the positive x-axis, unlike the MD simulations presented in section 2, where the cut was placed along the positive y-axis. This is done to follow the usual continuum mechanics convention, where the cut is usually placed along the x-axis (vid.[11, 1]), but it does not prejudice the comparison between continuum and atomistic results, as the cut surfaces can be obtained by performing the following change of coordinates, $x \mapsto -y$, $y \mapsto x$, as was described in table 1.

The solution procedure is the one originally outlined in [9]: the governing equation (eqn.9) is transformed employing the following Laplace transform in time:

$$\hat{u}_z(x, y, s) = \int_0^\infty u_z(x, y, t)e^{-st}\mathrm{d}t \tag{11}$$

followed by the two-sided Laplace transform in x:

$$U_z(\lambda, y, s) = \int_{-\infty}^\infty \hat{u}_z(x, y, s)e^{-\lambda s x}\mathrm{d}x \tag{12}$$

which results in the following differential equation in the compounded Laplace space:

$$\beta^2 s^2 U_z(\lambda, y, s) = \frac{\partial^2 U_z}{\partial y^2} \tag{13}$$

where $\beta^2 = b^2 - \lambda^2$. Assuming $U_z \to 0$ as $y \to \infty$, the general solution is:

$$U_z(\lambda, y, s) = C(\lambda, s)e^{-s\beta y} \tag{14}$$

By transforming the boundary condition (eqn.10), the form of U_z can be found:

$$U_z(\lambda, y, s) = \frac{B}{2\lambda s^2}e^{-s\beta y} \tag{15}$$

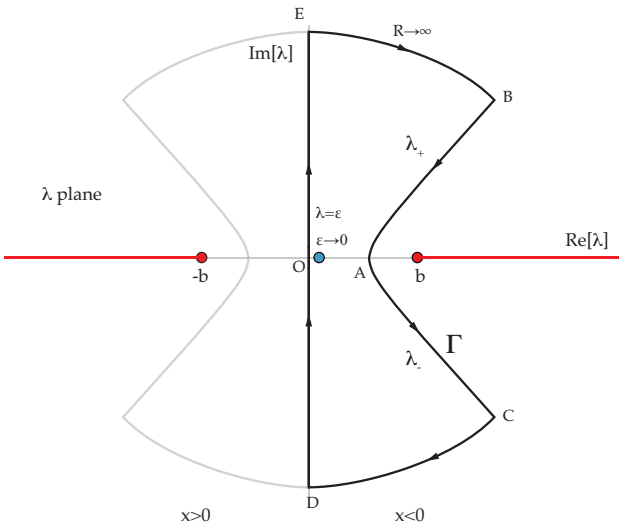

Figure 8: Integration path for eqn.16. The path for $x > 0$ has been faded for clarity.

The resulting stress field components due to the injection of a screw dislocation are given in table 1 (see [10] for details).

In the elastodynamic formulations of [10], [20], and [9] the displacement components were obtained by integration of the strain field components in real space. It is instructive to consider instead the direct inversion of U_z in eqn.15. The inversion in the spatial variable is as follows:

$$\hat{u}_z = \frac{1}{2\pi i}\int_{-i\infty}^{i\infty} \frac{B}{2\lambda s} e^{-s(\beta y - \lambda x)} \mathrm{d}\lambda \tag{16}$$

Eqn.16 prescribes an integration along the imaginary axis. It can be rewritten into a forward Laplace transform by employing the Cagniard-de Hoop technique. This requires distorting the integration path to

$$\tau = \beta y - \lambda x \tag{17}$$

Recalling that $\beta^2 = b^2 - \lambda^2$, and solving for λ to obtain:

$$\lambda_\pm = \frac{-\tau x \pm i y\sqrt{\tau^2 - b^2 r^2}}{r^2} \tag{18}$$

where $r = \sqrt{x^2 + y^2}$. Rewriting this as

$$\lambda_\pm = -X \pm iY, \quad \text{where} \quad X = \frac{\tau x}{r^2}, \quad Y = \frac{y\sqrt{\tau^2 - b^2 r^2}}{r^2} \tag{19}$$

It is found that $X = -\mathrm{Re}[\lambda]$ and $Y = \pm\mathrm{Im}[\lambda]$ are related as follows:

$$\left(\frac{X}{x}\right)^2 - \left(\frac{Y}{y}\right)^2 = \frac{b^2}{r^2}, \tag{20}$$

which is the equation of a hyperbola, see fig.8.

For $y > 0$, the λ_+ branch is in the upper half plane ($\mathrm{Im}[\lambda] > 0$), and the λ_- branch in the lower half plane ($\mathrm{Im}[\lambda] < 0$). The branches for which $\mathrm{Re}[\lambda] < 0$ (i.e., the left half plane) describe values of $x > 0$, and the branches for which $\mathrm{Re}[\lambda] > 0$ (i.e., the right half plane) describe those for which $x < 0$. Notice that these are all reversed for $y < 0$. Here the $y > 0$ case is discussed in detail.

The intersection of the hyperbola with the real axis is its vertex; it can be found by setting $\mathrm{Im}[\lambda_\pm] = Y = 0$. This occurs only when $\tau = br$. Thus, the vertex 'A' is found at

$$\lambda_A = -\frac{bx}{r}.$$

As λ_+ varies from λ_A towards the asymptote of the corresponding λ_+ branch, the value of τ varies from $\tau = br$ for λ_A to $\tau = +\infty$ when $\lambda_+ \to \lambda_B$, where point 'B' in fig.8 represents the asymptotic value of the hyperbola branch as $|\lambda_+| \to \infty$. This is the same for both $x > 0$ and $x < 0$. In the same way, the changes in the value of λ_- along the corresponding hyperbola branch entail variations in τ from $\tau = br$ at point 'A' to $\tau = +\infty$ at point 'C', where $|\lambda_-| \to \infty$; equally, this applies both for the $x > 0$ and $x < 0$ branches. Thus, the hyperbolic paths in the λ-plane map into a path along the real axis of the τ-plane, with $\tau \in [+br, \infty)$. It must be noted that when $x = 0$, $X = 0$ and both hyperbola branches collapse onto the imaginary axis; in that degenerate case $\tau = \beta y$. The path along these hyperbola branches is referred to as the *Cagniard path*.

The integrand in eqn.16 has branch cuts starting at $\lambda = \pm b$. The branch cuts are placed along the real axis at $\mathrm{Re}[\lambda] \in (-\infty, -b] \cup [b, \infty)$, as shown in fig.8. Note that $|\lambda_A| < b \; \forall x, y > 0$; thus the hyperbola never crosses the branch cuts as defined here. For convenience, the points $\lambda \to -i\infty$, $\lambda \to +i\infty$ and $\lambda = 0$ will be called, respectively, 'D', 'O' and 'E' as shown in fig.8.

The integrand in eqn.16 has a simple pole at $\lambda = 0$. This renders the integral in eqn.16 ill-defined because the integration contour can be defined in a number of ways. Stam (1990) [21] examined a mathematically analogous case arising when studying the radiation from a uniformly distributed load. For that case, Stam defined three different contours of integration depending on whether $x > 0$, $x < 0$ or $x = 0$, each avoiding the pole at $\lambda = 0$ in a different way depending on the value of x. Inspired by Feynman's propagator of a complex scalar field (cfr.[22]), a simpler approach is taken here, by displacing the pole an amount $\epsilon \in \mathbb{R}$ along the real axis as shown in fig.8. In this case, as $\epsilon \to 0$, the desired solution is recovered, and as guaranteed by the Sokhotski-Plemelj theorem, the integrals along the imaginary axis are guaranteed to exist in the sense of Cauchy principal values [23].

The resulting integrals can then be evaluated by considering a closed contour of integration Γ formed by the hyperbola branches, the imaginary axis, and two arcs of circumference of radius $R \to \infty$ for closure, as shown in fig.8. For $x > 0$, the resulting contour of integration is simply connected, so by Cauchy's theorem, the integral over such closed contour Γ is zero. For $x < 0$, the pole at $\lambda = \epsilon$ leaves a residue. Thus, it is found that (using a positive clock-wise contour convention):

$$I_\Gamma = \lim_{\epsilon\to 0}\left[I_{AC} + I_{CD} + I_{DO} + I_{OE} + I_{EB} + I_{BA}\right] = \begin{cases} 0 & x > 0 \\ 2\pi i \cdot \lim_{\epsilon\to 0} \mathrm{Res}[\lambda = \epsilon] & x < 0 \end{cases} \tag{21}$$

where each integral is described in the following.

First, the integrals along the Cagniard path are

$$I_{AC} + I_{BA} = \lim_{\epsilon\to 0} \frac{B}{4\pi i s} \int_{rb}^{\infty} \left[\frac{1}{(\lambda_- + \epsilon)} \frac{\partial \lambda_-}{\partial \tau} - \frac{1}{(\lambda_+ + \epsilon)} \frac{\partial \lambda_+}{\partial \tau}\right] e^{-s\tau} \mathrm{d}\tau \tag{22}$$

where $\frac{\partial \lambda_\pm}{\partial \tau}$ represents the Jacobian of the transformation of the integration variable from $\lambda_\pm$ to τ. Invoking Schwarz's reflection principle, one can show that

$$I_{AC} + I_{BA} = -\frac{B}{2\pi i s} \int_{rb}^{\infty} \mathrm{Im}\left[\frac{1}{\lambda_+} \frac{\partial \lambda_+}{\partial \tau}\right] e^{-s\tau} \mathrm{d}\tau \tag{23}$$

The integrals I_{CD} and I_{EB} can be proven to vanish at $R \to \infty$ as required by the Laplace transforms (cf.[9, 21]).

Finally, invoking the Sokhotski-Plemelj formula[23] for $\epsilon \to 0$,

$$I_{DO} + I_{OE} = \mathrm{P} \int_{-i\infty}^{i\infty} \frac{B}{4\pi i s} \frac{1}{\lambda} e^{-s(\beta y - \lambda x)} d\lambda \tag{24}$$

As for the residue, it can be computed as follows

$$\lim_{\epsilon\to 0} 2\pi i \mathrm{Res}[\lambda = \epsilon] = 2\pi i \lim_{\epsilon\to 0} \left[\lim_{\lambda\to\epsilon} (\lambda - \epsilon) \frac{B}{2s} \frac{1}{\lambda - \epsilon} e^{-s(y\sqrt{b^2 - \lambda^2} - \lambda x)}\right] = 2\pi i \frac{B}{2s} e^{-sby} \tag{25}$$

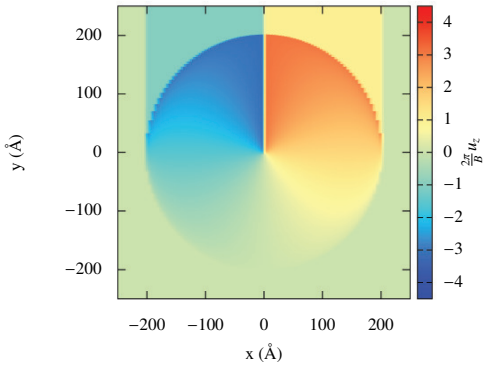

Figure 9: The u_z displacement field showing the emissions.

Thus,

$$\mathrm{P}\int_{-i\infty}^{i\infty}\frac{B}{4\pi i s}\frac{1}{\lambda}e^{-s(\beta y-\lambda x)}d\lambda=\frac{B}{2\pi i s}\int_{rb}^{\infty}\mathrm{Im}\left[\frac{1}{\lambda_+}\frac{\partial\lambda_+}{\partial\tau}\right]e^{-s\tau}\mathrm{d}\tau+\frac{B}{2s}e^{-sby}\mathrm{H}(x) \tag{26}$$

Where the Cauchy principal value on the left hand side of the equation represents $\hat{u}_z$. The $\mathrm{H}(x)$ accounts for the fact that the pole's residue only acts for $x>0$.

The case for which $y<0$ results in an analogous construction, but the signs of $\lambda_\pm$ are swapped, so in order to keep the clock-wise positive circulation criterion one must invert the sign of the residue. Thus,

$$\hat{u}_z=\frac{B}{2\pi i s}\int_{rb}^{\infty}\mathrm{Im}\left[\frac{1}{\lambda_+}\frac{\partial\lambda_+}{\partial\tau}\right]e^{-s\tau}\mathrm{d}\tau+\mathrm{sign}(y)\frac{B}{2s}e^{-sby}\mathrm{H}(x) \tag{27}$$

This must be now be inverted in time. The pole's contribution can be found immediately by inspection:

$$i_{\mathrm{residue}}=\mathrm{sign}(y)\frac{B}{2}\mathrm{H}(t-by)\mathrm{H}(x)\mathrm{H}(-t+br) \tag{28}$$

where $\mathrm{H}(-t+br)$ has been added to account for the fact that since it is part of the hyperbolic branching, the pole only acts for $t\equiv\tau\in[+br,\infty)$.

The other integral can also be obtained immediately by inspection. Invoking the Bromwich integral, its time inverse will be

$$i_{\mathrm{Cagniard}}=\frac{1}{2\pi i}\int_{\mathrm{Br}}\mathrm{d}s e^{s\tau}\left[\frac{B}{2\pi i s}\int_{rb}^{\infty}\mathrm{Im}\left[\frac{1}{\lambda_+}\frac{\partial\lambda_+}{\partial\tau}\right]e^{-s\tau}\mathrm{d}\tau\right]=\frac{1}{2\pi i}\int_{\mathrm{Br}}\mathrm{d}s e^{s\tau}\left[\frac{B}{2\pi i s}\int_{0}^{\infty}\mathrm{H}(\tau-br)\mathrm{Im}\left[\frac{1}{\lambda_+}\frac{\partial\lambda_+}{\partial\tau}\right]e^{-s\tau}\mathrm{d}\tau\right]=$$
$$=\frac{1}{2\pi i}\mathrm{H}(t-br)\mathrm{Im}\left[\frac{1}{\lambda_+}\frac{\partial\lambda_+}{\partial t}\right] \tag{29}$$

This can be shown to yield:

$$u_z(x,y,t)=\frac{B}{2\pi}\arctan\left(\frac{-tx}{-y\sqrt{t^2-b^2\left(x^2+y^2\right)}}\right)\mathrm{H}(t-br)+\mathrm{sign}(y)\frac{B}{2\pi}\mathrm{H}(t-by)\mathrm{H}(x)\mathrm{H}(-t+br) \tag{30}$$

As stated above, here the cut is placed along the x-axis. Since in the MD simulations the cut will typically be placed along the y-axis, it is more convenient to express the fields by swapping $x\mapsto -y, y\mapsto x$ (as shown in table 1), i.e., as

$$u_z(x,y,t)=\frac{B}{2\pi}\arctan\left(\frac{-ty}{x\sqrt{t^2-b^2\left(x^2+y^2\right)}}\right)\mathrm{H}(t-br)+\mathrm{sign}(x)\frac{B}{2\pi}\mathrm{H}(t-bx)\mathrm{H}(-y)\mathrm{H}(-t+br) \tag{31}$$

In either case, the pole introduces a wave emission along the cut surface, propagating outwards in the direction perpendicular to it; this wavefront, emitted from the cut surface and in parallel to it, corresponds with the *emission* reported in the MD simulations of section 2. The emission can be appreciated in fig.9, which shows the u_z field for the cut along the positive y-axis.

The justification for the emission is found in the boundary condition given by eqn.10: were the solution to lack the emission term and consist only of the radial term obtained from the Cagniard path, then the boundary condition would only be satisfied for $x < t/b$, rather than for all $x > 0$ (i.e., along the whole cut surface). The emission is the occurs because of the presence of the pole at $\lambda = 0$, which does not appear when deriving the stress fields (vid.[10, 9]), so it does not affect the stress field components. Furthermore, upon the injection of a dipole, the emission term of one dislocation ought to cancel with the other's. However, as was shown in fig.6, the emission is present in the atomistic injection process, and produce unexpected features in the stress fields, which can only be understood in terms of the many simplifications introduced in modelling the injection process in the continuum.

The fundamental assumptions of this model, which Gurrutxaga-Lerma et al. (2015) [10] showed to converge to the traditional, time-independent fields of screw dislocations [1], are two: (1) that the core is infinitely thin—and can therefore be modelled via the H(x) Heaviside step function in eqn.10; and (2) that the injection occurs instantaneously—and can therefore be modelled via the H(t) Heaviside function in eqn.10. These two assumptions are justified within the D3P framework they were developed for: an infinitely thin core, albeit unrealistic, is a reasonable assumption if only the long-range interactions are required to account for plasticity (cf.[1]); the sudden injection is reasonable if the injected dislocation is used as a device to model injections from crack tips and surfaces, reversals of motion, or dislocation monopoles [7].

However, neither are exactly true in an atomistic representation of dislocations. In the following section, various ways of representing the boundary condition in eqn.10 in a molecular dynamics (MD) simulation are discussed, and its implications for continuum model is analysed.

5. Advanced continuum models of the injection of a screw dislocation

The MD simulations presented in section 3 display a series of characteristics missing in the original derivation of the fields of an injected, quiescent screw dislocation given in section 4. As has been discussed in section 3, these must be attributed to atomistic effects missed in the continuum description of an injection.

Firstly, no strong singularities in the elastodynamic fields are observed at the wave fronts. This is likely because in the atomistic simulations the displacement across the cut has to be accumulated gradually over time, from zero to the final Burgers vector of the screw dislocation; as has been explained in section 2.3.2, the dislocation is not injected otherwise.

Secondly, that the emission along the cut surface in the u_z displacement field is present in both the MD and the elastodynamic descriptions, but as can be observed in figs.6e and 6f, there is also an emission in u_x and u_y missed in the latter. The emission in u_x clearly propagates at the longitudinal speed of sound (see fig.6e), whilst the emission in u_y propagates at the lower transverse speed of sound (see fig. 6f). This suggests that the atomistic injection induces atomic displacements along the cut surface both in u_y and u_x, which are not present in the continuum description given in section 4.

In this section, it is argued that both features can in fact be accounted for employing more sophisticated descriptions of the injection process in the elastodynamic continuum. The classical continuum account of an injection, provided in section 4, is based on the boundary condition given by eqn.10. This condition describes the sudden injection of a screw dislocation the core of which is modelled as a Volterra discontinuity with no spatial width. As has been highlighted by the molecular dynamics simulations, both the sudden injection assumption and the lack of a core width are unrealistic. Provided that adequate boundary conditions are introduced, it will be shown that the main features observed in the MD simulations can be modelled in the continuum, and therefore interpreted as such.

5.1. Ramping up the injection of screw dislocation

A more accurate description of the injection process, as highlighted by the MD simulations, can be achieved by ramping up the injection of the screw dislocation.

Following eqn.51, the governing equation is:

$$u_{z,xx} + u_{z,yy} = b^2 u_{z,tt}$$

The usual boundary condition (sudden injection), is:

$$u_z(x, 0, t) = \frac{B}{2} \cdot \mathrm{H}(x) \cdot \mathrm{H}(t)$$

meaning that for $x > 0$ (i.e., the cut) and for $t > 0$ a displacement of magnitude B is imposed. The molecular dynamics have shown that in the atomistic description, the disregistry cannot be imposed instantaneously.

Albeit the continuum description has no way of identifying this feature—i.e., the continuum will not detect this feature , it can still model it by 'ramping up' the injection in time as follows

$$u_z(x, 0, t) = B \cdot \mathrm{H}(x) \cdot \mathrm{R}(t) \tag{32}$$

where, as a first approach approximation, $R(t)$ is given by equation 7. This boundary condition will gradually inject a partial dislocation into the system, up to the magnitude of the Burgers vector. The core structure, however, remains infinitely thin.

5.1.1. Solution to the ramped injection

This problem can be solved analytically. Using the standard solution method described for instance in [7, 10], two successive Laplace transforms are applied over the governing equation 51 to obtain

$$U_z(\lambda, y, s) = C(s, \lambda) e^{-s\beta y} \tag{33}$$

where $C(s, \lambda)$ is obtained from transforming the boundary condition, in this case eqn.32:

$$\mathcal{L}_x\{\mathcal{L}_t\{B\mathrm{H}(x)R(t)\}\} = B\mathcal{L}_x\{\mathrm{H}(x)\}\mathcal{L}_t\{R(t)\} \tag{34}$$

where

$$\mathcal{L}_x\{\mathrm{H}(x)\} = \lambda s$$

$$\begin{aligned} \mathcal{L}_t\{R(t)\} = \int_0^\infty R(t) e^{-st} \mathrm{d}t &= \int_0^{\tau_0} \frac{t}{\tau_0} e^{-st} \mathrm{d}t + \int_{\tau_0}^\infty e^{-st} \mathrm{d}t \\ &= \frac{1 - e^{-s\tau_0}}{s^2 \tau_0} \end{aligned} \tag{35}$$

So

$$U_z(\lambda, y, s) = \frac{B}{\lambda s^3 \tau_0} (1 - e^{-s\tau_0}) e^{-s\beta y} \tag{36}$$

The presence of the pole at $\lambda = 0$ suggest that, as in section 4, an emission term will be present in u_z as required to satisfy the boundary condition for all values of x across the cut surface. Since that case was already mathematically studied in 4, here for simplicity, consider $\sigma_{xz} = \mu u_{z,x}$. Its transform:

$$\Sigma_{xz} = \frac{\mu B}{\tau_0 s^2} e^{-s\beta y} - \frac{\mu B}{\tau_0 s^2} e^{-s(\beta y + \tau_0)} \tag{37}$$

Both terms are of the same form, only that the second one entails a time delay, due to the τ_0 in the kernel.

Using Cagniard-de Hoop, one can invert the first term in the right hand side of eqn.37 as follows. Let:

$$\hat{\sigma}_{xz_I} = \frac{1}{2\pi i} \int_{-i\infty}^{i\infty} \frac{\mu B}{\tau_0} \frac{1}{s} e^{-s(\beta y - \lambda x)} d\lambda \tag{38}$$

Defining $\tau = \beta y - \lambda x$ and distorting the integration path, leading to

$$\hat{\sigma}_{xz_I} = \frac{\mu B}{2\pi\tau_0}\frac{1}{s}\int_0^\infty \mathrm{H}(\tau - rb)\mathrm{Im}\left[\frac{\partial\lambda_+}{\partial\tau}\right]e^{-s\tau}\mathrm{d}\tau \tag{39}$$

So the Bromwich integral is

$$\sigma_{xz_I} = \frac{1}{2\pi i}\int_{\mathrm{Br}}\frac{\mu B}{2\pi\tau_0}\left(\frac{1}{s}\cdot\int_0^\infty \mathrm{H}(\tau - rb)\mathrm{Im}\left[\frac{\partial\lambda_+}{\partial\tau}\right]e^{-s\tau}\right)e^{st}ds \tag{40}$$

Define

$$f(t) = \mathrm{H}(t - rb)\mathrm{Im}\left[\frac{\partial\lambda_+}{\partial t}\right] \tag{41}$$

Then by properties of the Laplace transform the stress field can be obtained as the following convolution:

$$\sigma_{xz_I} = \frac{\mu B}{2\pi\tau_0}\int_0^t f(\tau)\mathrm{H}(t-\tau)\mathrm{d}\tau \tag{42}$$

The second term is obtained in the same way, only that the τ_0 imposes a delay factor throughout:

$$\sigma_{xz_I} = \frac{\mu B}{2\pi\tau_0}\int_0^{t-\tau_0} f(\tau)\mathrm{H}(t-\tau)\mathrm{d}\tau \tag{43}$$

The convolution is immediate; for $\tau < rb$ the integrand it is zero. For $\tau > rb$ the integrand is just $\mathrm{Im}\left[\frac{\partial\lambda_+}{\partial t}\right]$ because $\mathrm{H}(t-\tau) = 1$ throughout as guaranteed by the integration limit. Thus

$$\sigma_{xz_I} = \frac{\mu B}{2\pi\tau_0}\frac{y\sqrt{t^2 - b^2r^2}}{r^2}\mathrm{H}(t - br) \tag{44}$$

Whereby, compounding the solution,

$$\sigma_{xz} = \frac{\mu B}{2\pi\tau_0}\left[\frac{y\sqrt{t^2 - b^2r^2}}{r^2}\mathrm{H}(t - br) - \frac{y\sqrt{(t-\tau_0)^2 - b^2r^2}}{r^2}\mathrm{H}((t-\tau_0) - br)\right] \tag{45}$$

The asymptotic limit of this expression when $t \to \infty$ is the same as that of a sudden injection (i.e., the quasi-static field), and when $\tau_0 \to 0$, it matches the sudden injection solution provided in table 1. It is worth noticing that the base solution (eqn.44) is the antiderivative in time of the suddenly injected dislocation's field, whereas the actual solution (eqn.45), where the second term is incremented in time via the $t - \tau_0$ factor, is the discretised approximation of a derivative. Thus, in the $\tau_0 \to 0$ limit, σ_{xy} is, the definition of a derivative in time, and one that matches the sudden injection's field.

The solution to σ_{xz} and all other stress, displacement and strain components is obtained similarly. In particular, the displacement field entails that the emission term becomes ramp-like:

$$u_{z_{\mathrm{emission}}}(x, y > 0, t) = \frac{B}{2\pi\tau_0}\left((t - by)\mathrm{H}(t - by) - (t - \tau_0 - by)\mathrm{H}(t - \tau_0 - by)\right) \tag{46}$$

The displacement emission along the cut surface does not introduce strong spatial gradients other than for an very thin discontinuity between $t = by$ and $t - \tau_0 = by$. This is in fact already accounted for in the analytic forms of the stress fields provided above.

It is clear that the sudden injection (given in eqn.10) displays a square root singularity at the injection front, which is not present in the ramped up injection. This defines the ramped up injection as a smoother process, in agreement with the molecular dynamics simulation where no strong discontinuities at the injection fronts are observed. In all cases the elastodynamic fields are almost identical to the sudden injection's for short timescales (i.e., $\tau_0 < 1$ps), as is shown in fig.10a and 11b. However, the ramped injection cannot by construction display any emission from the cut plane in u_x and u_y, unlike what was shown in the MD simulation. Hence, further considerations are needed.

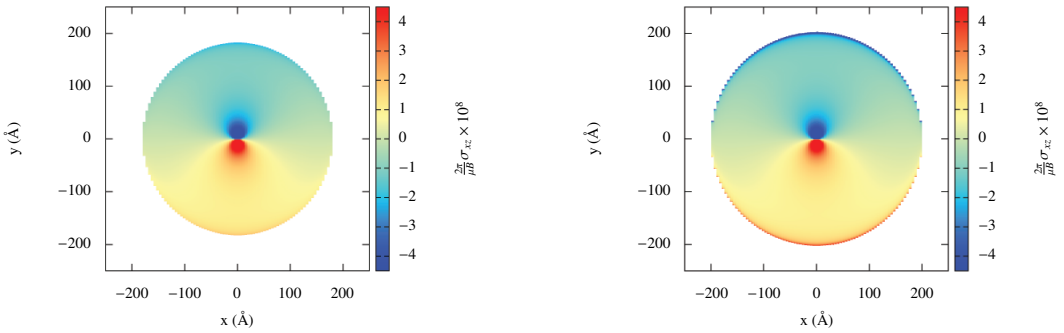

(a) Ramped injection

(b) Sudden injection

Figure 10: Injection of a screw dislocation. Notice the lack of singularities at the injection front for the case of the ramped injection.

5.2. *Spreading out the core*

Ramping up the injection helps in understanding the lack of strong singularities at the injection fronts observed in the molecular dynamics simulations, but it does not reproduce any of the additional features observed in them.

The Volterra dislocation's core invoked so far has no width, which is not representative of atomistic reality; for instance, it is well-known that the core of screw dislocations in BCC materials is non-planar [24, 12]. Even before achieving such detailed resolution, more sophisticated continuum models such as the Peierls-Nabarro model [25, 26] already assume the core has a finite width. As a first approximation to help in building understanding of what a finitely wide core would entail in this context, rather than employing the more sophisticated Peierls-Nabarro description, a simple spread out ramp core of width δ will be employed here, where the function $R(x)$ describes its spatial width as follows

$$R(x) = \begin{cases} 0 & x < -\delta/2 \\ x/\delta + 1/2 & -\delta/2 < x < \delta/2 \\ 1 & x > \delta/2 \end{cases}, \tag{47}$$

whereby the boundary condition is now

$$u_z(x, 0, t) = \frac{B}{2} R(x) \mathrm{H}(t) \tag{48}$$

A general formulation for the solution of this problem, reliant on the Cagniard-de Hoop technique, can be found in [27]. The procedure itself is analogous to the one employed in section 5.1 for the solution of the ramped dislocation that, for brevity, it will not be reproduced here.

One can verify that, for instance

$$\sigma_{yz} = \frac{\mu B}{2\delta\pi} \left(\tanh^{-1} \left(\frac{\sqrt{t^2 - b^2\left((\delta/2 + x)^2 + y^2\right)}}{t} \right) \cdot H\left(t - b\left((x + \delta/2)^2 + y^2\right)^{1/2}\right) \right.$$
$$\left. - \tanh^{-1} \left(\frac{\sqrt{t^2 - b^2\left((x - \delta/2)^2 + y^2\right)}}{t} \right) \right) \cdot H\left(t - b\left((x - \delta/2)^2 + y^2\right)^{1/2}\right) \tag{49}$$

This field has the right asymptotic behaviour both when $\delta \to 0$ and when $t \to \infty$. The same process, applied to the

The resulting σ_{yz} field component is shown in fig.11a. As was advanced in the previous section, the injection of a spread out core does not bear any singularities at the front — it is a smooth process, with no emission along the cut surface. Were the injection to be ramped with $R(t)$ defined rather than sudden with $\mathrm{H}(t)$, the solution would be the

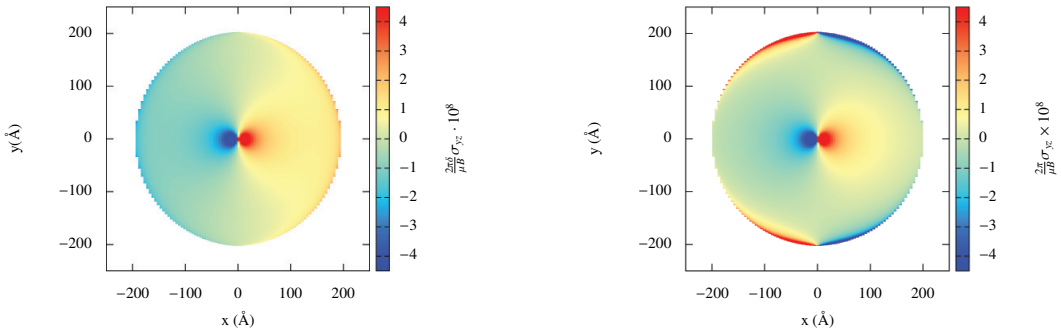

(a) Spread out core model

(b) Sudden injection, Volterra core

Figure 11: σ_{yz} stress field component at $t = 7ps$ for tungsten, for the case of a spread out core with a sudden injection.

following:

$$\sigma_{yz} = \frac{\mu B}{4\delta\pi\tau_0}\Bigg[\sqrt{4t^2 - b^2\left(d^2 + 4dx + 4\left(x^2 + y^2\right)\right)} + \sqrt{4t^2 - b^2\left(d^2 - 4dx + 4\left(x^2 + y^2\right)\right)}$$
$$-2t\tanh^{-1}\left(\frac{\sqrt{t^2 - b^2\left(\left(\frac{d}{2} + x\right)^2 + y^2\right)}}{t}\right) - 2t\tanh^{-1}\left(\frac{\sqrt{t^2 - b^2\left(\left(x - \frac{d}{2}\right)^2 + y^2\right)}}{t}\right)$$
$$+\Bigg(-\sqrt{4(t-\tau_0)^2 - b^2\left(d^2 + 4dx + 4\left(x^2 + y^2\right)\right)} + \sqrt{4(t-\tau_0)^2 - b^2\left(d^2 - 4dx + 4\left(x^2 + y^2\right)\right)} +$$
$$2(t-\tau_0)\tanh^{-1}\left(\frac{\sqrt{(t-\tau_0)^2 - b^2\left(\left(\frac{d}{2} + x\right)^2 + y^2\right)}}{t-\tau_0}\right) - 2(t-\tau_0)\tanh^{-1}\left(\frac{\sqrt{(t-\tau_0)^2 - b^2\left(\left(x - \frac{d}{2}\right)^2 + y^2\right)}}{t-\tau_0}\right)\Bigg)\Bigg]$$

It can be shows that this kind of injection still entails an emission along the cut surface in the u_z but, again by construction, fails to capture the additional emissions in u_y and u_x. It follows that the main characteristic of the atomistic injection that these models fail to capture is the emission in u_y and u_x along the slip surface. This can be attributed to the failure of the continuum models so far to adequately model the structure of the injected core. In the molecular dynamics description, the dislocation is injected gradually by slipping a half plane of atoms with respect to another along the cut surface until the required Burgers vector wide disregistry is achieved. In doing so, the atomic plane will be translated along non-lattice positions; this transient mismatch will cause a temporary stacking fault in the atomic planes, which is translated in the appearance of atomic displacements exerted upon the nearby atomic rows. The result is the sudden emission along the cut surface observed in molecular dynamics. Because the continuum description provided hitherto assumes the cut is performed along perfectly flat surfaces, this emission remains missing.

This effect can only be observed a priori employing atomistic effects. It highlights that the unidimensional core description provided by infinitely thin cores or ramp cores employed here and, by extension, by more sophisticated models as would be the dynamic Peierls-Nabarro model, miss in-plane core effects. This does not mean that one cannot model some of the latter ad hoc, by explicitly forcing an emission along the cut surface, in the positive half space. This is done in the following section.

5.3. The emission along the cut surface

The additional in-plane emissions in u_x and u_y along the cut can be regarded as the result of the injection process, which in the atomistic case is performed by slipping an atomic plane with respect to another along the cut surface. Since this process is gradual, the sliding atoms at the interface will temporarily find themselves in non-equilibrium lattice positions, thereby experiencing a net force of displacement both in the u_x and u_y components observed in the atomistic simulations. Once the final, lattice position is reached, these additional displacements should disappear, as is suggested by the molecular dynamics: once the injection is completed, the emissions in u_x and u_y vanish, whilst that in u_z, the only one predicted in the continuum, remains.

This process can be modelled in the continuum as well. Following the atomistic simulations presented in section 2, the process can be modelled by considering transient displacement boundary conditions in u_x and u_y, such that they gradually increase to a certain maximum displacement Δ to then decrease and vanish once the atomic planes have reached a fully lattice position.

Although the specification of these displacement boundary conditions are a matter of atomistic detail, the process can be approximated faithfully by modelling it as a sinusoidal displacement. For instance, if the injection takes place over a time step of magnitude τ_0, for u_x this could be

$$u_x(0, y, t) = \begin{cases} \Delta_x \sin\left(\frac{2\pi t}{\tau_0}\right) & 0 < t < \frac{\tau_0}{2} \\ 0 & t > \frac{\tau_0}{2} \end{cases} \tag{50}$$

where Δ_x is the amplitude of the maximum displacement. This displacement is applied everywhere across the cut surface, and it is like introducing an edge dislocation in the first quarter period and then removing it in the second quarter period. An analogous boundary condition can be introduced for u_y.

The resulting mathematical problem can be tackled in a number of ways. Here, as a first approach approximation, the in-plane emissions are modelled as sudden steps of magnitude Δ_x and Δ_y in u_x and u_y respectively, which are applied on the whole cut surface. For a more general form of u_x and u_y such as that given in eqn.50, the convolution theorem for Laplace transforms can be applied to find the solution [28]. Still, the fundamental feature of these solutions, namely the emission along the cut surface, can be captured by considering the simple

5.3.1. Emissions in u_x

Given the governing equations (q.v.[28])

$$\begin{aligned} \phi_{,xx} + \phi_{,yy} &= a^2 \phi_{,tt} \\ \psi_{,xx} + \psi_{,yy} &= b^2 \psi_{,tt}, \end{aligned} \tag{51}$$

the emission along the cut surface can be modelled, as a first approach approximation, as resulting from the application of a sudden distributed displacement along the positive y-axis.

For simplicity, the general problem of an arbitrary distributed displacement with both u_x and u_y non-zero components can in principle be solved as the superposition of two problems: one consisting on a distributed u_x displacement of a certain magnitude Δ_x with an accompanying $u_y = 0$; and one consisting of a distributed u_y displacement of a certain magnitude Δ_y with an accompanying $u_x = 0$. As a first approach approximation, the applied displacements are applied suddenly but their effect remains constant. It is then easy to cancel their effect by applying at a later time, a displacement of opposite magnitude. A more sophisticated approach would provide a time-dependent description of the magnitude of these displacements, reflecting the atomistic displacements the actual injection process entails.

Thus,

$$u_x(x = 0, y, t) = \Delta_x \mathrm{H}(y)\mathrm{H}(t), \tag{52}$$

$$u_y(x = 0, y, t) = 0 \tag{53}$$

where Δ_x is the magnitude of the applied displacement, and such that

$$u_x = \phi_{,x} - \psi_{,y}, \qquad u_y = \phi_{,y} + \psi_{,x} \tag{54}$$

Define the following Laplace transforms:

$$\hat{f}(x,y,s) = \mathcal{L}_t\{f(x,y,t)\} = \int_0^\infty f(x,y,t)e^{-st}\mathrm{d}t \tag{55}$$

$$F(x,\lambda,s) = \mathcal{L}_y\{\hat{f}(x,y,s)\} = \int_{-\infty}^\infty \hat{f}(x,y,s)e^{-\lambda sy}\mathrm{d}y \tag{56}$$

Applying these transforms to the governing eqn.51, their solution in Laplace space is the usual

$$\Phi(x,\lambda,s) = C_\phi(\lambda,s)e^{-s\alpha x} \tag{57}$$

$$\Psi(x,\lambda,s) = C_\psi(\lambda,s)e^{-s\beta x} \tag{58}$$

where $\alpha^2 = a^2 - \lambda^2$ and $\beta^2 = b^2 - \lambda^2$, and where the value of C_ϕ and C_ψ can in principle be found from the boundary conditions.

Applying the same transforms to the boundary conditions eqns.52 and 63,

$$U_x(0,\lambda,s) = \frac{\Delta_x}{\lambda s^2} = -s\alpha C_\phi - s\lambda C_\psi \tag{59}$$

and

$$U_y(0,\lambda,s) = 0 = s\lambda C_\phi - s\beta C_\psi \tag{60}$$

This leads to the following system of equations:

$$\begin{pmatrix} -s\alpha & -s\lambda \\ s\lambda & -s\beta \end{pmatrix} \cdot \begin{pmatrix} C_\phi \\ C_\psi \end{pmatrix} = \begin{pmatrix} \frac{\Delta}{\lambda s^2} \\ 0 \end{pmatrix}, \tag{61}$$

The solution to this system of equations is detailed in the Appendix A. There, it is shown that for the u_x displacement the solution takes the form of

$$u_x = \int_0^t \mathrm{Im}\left[\frac{\alpha\beta\Delta_x}{\lambda_+(\alpha\beta+\lambda_+^2)}\frac{\partial\lambda_+}{\partial\tau}\right]_a \mathrm{H}(\tau - ra)\mathrm{H}(t-\tau)\mathrm{d}\tau + \int_0^t \mathrm{Im}\left[\frac{\lambda_+\Delta_x}{\alpha\beta+\lambda_+^2}\frac{\partial\lambda_+}{\partial\tau}\right]_b \mathrm{H}(\tau - rb)\mathrm{H}(t-\tau)\mathrm{d}\tau + \mathrm{sign}(y)\Delta_x\mathrm{H}(t-ax) \tag{62}$$

where $\lambda_+ = \frac{-\tau y + ix\sqrt{t^2-a^2r^2}}{r^2}$.

The two integrals in eqn.62 describe displacement fields radiated from the origin at $x = 0, y = 0$; crucially however, the last term describes an emission of magnitude Δ_x perpendicular to the cut surface, and propagating at the longitudinal speed of sound. This shows that a displacement boundary condition in u_x entails a longitudinal emission, in agreement with what was observed in the molecular dynamics simulations in section 2. If at some time $t = \tau_0 > 0$ an additional boundary condition such as $u_x(x = 0, y, t) = -\Delta_x\mathrm{H}(y)\mathrm{H}(t-\tau_0)$ were applied, the resulting wave emissions would cancel each other. This would represent the cut surface reaching its lattice position again. Otherwise, as was suggested above, one may use the solutions derived here to, by convolution in the spatial Laplace transform (vid.[28]), reach a solution for any other boundary condition in u_x. In either case, an emission will be present.

The same kind of derivation may be applied for a u_y displacement step. In that case, the boundary conditions would be

$$u_x(x = 0, y, t) = 0 \tag{63}$$

$$u_y(x = 0, y, t) = \Delta_y\mathrm{H}(y)\mathrm{H}(t) \tag{64}$$

One will reach, through analogous means, an emission term along the cut, of the form

$$u_{y_{\mathrm{emission}}} = \mathrm{sign}(y)\Delta_y\mathrm{H}(t - bx) \tag{65}$$

which propagates outward from the cut surface at the transverse speed of sound. The solution also consists of a term radiating from the origin, which is not reproduced here due to its length. Both radial terms over u_x and u_y are emitted from the core at $x = 0, y = 0$.

6. Comparison between MD results and advanced continuum models

Reconsider now the comparison between the MD simulation results and the advanced continuum models outlined in section 5. By assuming that the dislocation can be represented by a jump, sudden or spread over a localised region of space in the u_z displacement component alone, the continuum model will invariably miss additional features that can only be captured in the atomistic simulations: in this case, that if a dislocation is to be generated anew, the atoms in the slipped region will take a finite time to reach their lattice position, and meanwhile will experience out-of-plane displacements (or forces) that entail that the core of the screw dislocation can only be properly represented through boundary conditions both in u_z, as it is usually done, and in u_x and u_y. As has been shown in section 5.3, even the simple assumption that there exists a homogeneous distributed displacement applied over the cut surface is able to reproduce the basic feature observed in the atomistic case: an outward radiation from the slipped surface both in u_x and u_y. A more sophisticated description ought to take into account the variation in time of the magnitude of such applied components, which should be motivated by the way the injection takes place.

However, as they stand the continuum models presented in section 5 do not predict stress emissions of the magnitude showcased by the atomistic simulations, as seen in fig.6b. These stress waves emerge due to the non-instantaneous nature of the injection mechanism and disappear again after the atoms near the cut-plane have rearranged themselves back into lattice positions. Given that the gradual injection inevitably gives rise to these stress bands near the cut-plane in a real lattice structure, it can be concluded that these atomic rearrangement stresses are physical rather than a shortcoming of the MD simulation. From fig.6 it can be seen that the magnitude of these stress bands are comparable to the stresses at the dislocation core. Due to their extended nature throughout half the system, it is to be expected that these stress waves will dominate the transient behaviour of the elastodynamic fields, which cause reflections and disturb the system considerably compared the continuum predictions. Only once these waves have been dissipated by the damping layer, observed for $t > 50ps$, does the system recover elastic fields in good agreement with the continuum equivalent. These stress waves seem to correspond to the u_x and u_y displacements, which can be seen to be highly non-planar at the same locations, and suggest that their modelling in section 5.3 as planar waves is insufficient, and more sophisticated models will be needed to produce an appropriate continuum representation of this effect. In the molecular dynamics simulations, attempts were made to minimise the magnitude of these stress bands by varying the core shape and thickness of the fixed region. None of these injection attempts resulted in a screw dislocation and even if one were to be successful, the stress bands would still be present and only their magnitude would be reduced.

Thus, the continuum model can successfully reproduce the most relevant features of the atomistic models. An adequate modelling of the core (see sections 5.1.1 and 5.2) has been shown to induce a smoother injection, thereby helping understand the lack of strong singularities in the atomistic simulations. The emission in u_z has been shown to be present in the continuum description of injection process (see section 4). The additional emissions in u_x and u_y have been modelled as sudden applied displacements over the cut surface, leading to emission terms that, as is observed in the molecular dynamics, propagate at the longitudinal and transverse speed of sound respectively, and are more or less of constant magnitude. The simplified modelling of these emissions explains why the continuum fails to predict corresponding emissions in stress, and suggest that the evolution of the core structure and the cut surface as the injection takes place requires a three dimensional treatment of the screw dislocation's core, involving displacement boundary conditions in u_z and also in u_x and u_y.

7. Conclusions

This article shows that injection of screw dislocations in MD simulations can only be achieved by a gradual injection process in order to satisfy their associated topology. Comparison with the corresponding elastodynamic description of the injection of straight screw dislocations has highlighted a number of common features, but also a number of discrepancies. Firstly, the predicted divergences at the elastodynamic fields wave fronts were not observed in the MD simulation. Secondly, an emission along the entire cut plane in both displacement and stress fields was observed. Finally, the in-plane displacement field components were shown not to vanish as a result of in-plane atomic rearrangements in the vicinity of the cut plane.

Crucially, the elastodynamic model assumes that the injection is instantaneous, and that the dislocation's core structure is infinitely thin and unidimensional (i.e., dependent on a single displacement component). The consequences of these assumptions explain all the discrepancies between the atomistic and elastodynamic models. First,

an instantaneous injection entails a strong discontinuity at the injection fronts, but upon deriving the elastodynamic fields of a screw dislocation the Burgers vector of which is gradually built up in time, it was shown that the injection becomes a smooth process. This brings the MD simulations and continuum descriptions in better agreement with one another. Further to this, assigning the core a finite width also resulted in a smoother injection. Second, the emission along the entire cut plane was shown to be a hitherto overlooked feature of the out-of-plane displacement component, the magnitude of which was shown to be comparable to that observed in the MD simulations.

Finally however, neither the emission in the out-of-plane component nor the smoother injection process could explain the presence of non-zero in-plane displacement components. These were attributed to the atomistic injection process, where the atomic planes along the cut surface must be displaced through non-lattice positions before the final, Burgers vector wide lattice position is achieved. These non-lattice positions induce in-plane displacements that, as was observed in the MD simulations, vanish once the injection is complete, but that meanwhile will manifest as emissions affecting both the in-plane displacement components and the corresponding stress field components.

By showing that these emissions cannot be explained by providing the continuum core with a finite width, nor by making the injection process gradual, this article has highlighted the need for a fully three-dimensional model of the core of an injected dislocation. As a first approach approximation, the problem of a distributed in-plane displacement applied over an elastodynamic half-space has been solved, showing that modelling the emissions in u_x and u_y as the result of a distributed displacement applied over the cut surface leads to emissions that have all the adequate features. Thus, this work has highlighted the truly three-dimensional nature of the core of a screw dislocation by means of exploring its injection process. Albeit the injection can be modelled in the continuum as a Volterra dislocation that is suddenly injected into the system (as had been proposed by Markenscoff (1980) [9] and Gurrutxaga-Lerma et al. (2015) [10]), in-plane effects are missed in this description, and can only be found, as was done here, by proper study of the atomistic effects involved in the injection of a screw dislocation.

The elastodynamic framework presented here can therefore be used to interpret the atomistic effects described in this work: the additional core effects have been modelled as additional displacement disturbances arising from the injection process, and explained as such. This process can only properly be described by employing atomistic simulations, and would otherwise be missed in the continuum description of the injection of a screw dislocation. Thus, as has been shown in this article, one can envision a multiscale hierarchical approach whereby the atomistic simulations of the injection can be employed to inform the elastodynamic description of the injection. This approach enables the inherently atomistic features of dislocation injection processes to be incorporated into a continuum theory in order to benefit from the much greater length and time scales inherent to a continuum description.

Acknowledgements and contributions

JV was supported through a studentship in the Centre for Doctoral Training on Theory and Simulation of Materials at Imperial College funded by EPSRC under Grant No. EP/L015579/1. BGL acknowledges support by the EPSRC under the EPSRC Doctoral Prize Fellowship scheme.

JV developed and carried out the MD simulations. BGL conceived the mathematical models. JV and BGL wrote the paper. DSB, DD and APS supervised the work and contributed to the writing of the discussions.

The authors report no competing interests. This work did not involve any collection of human or animal data. This work does not have any experimental data. All simulation results are made available upon request to the corresponding author.

References

[1] J. P. Hirth and J. Lothe. *Theory of dislocations*. Krieger Publishing Company, 2nd edition, 1992.

[2] D. Hull and D. J. Bacon. *Introduction to Dislocations*. Butterworth-Heinemann, Oxford, UK, 5th edition, 2011.

[3] E. M. Bringa, K. Rosolankova, R. E. Rudd, B. A. Remington, J. S. Wark, M. Duchaineau, D. H. Kalantar, J. Hawreliak, and J. Belak. Shock deformation of face-centred-cubic metals on subnanosecond timescales. *Nature materials*, 5(10):805–809, 2006.

[4] A. Gouldstone, K. J. Van Vliet, and S. Suresh. Nanoindentation: Simulation of defect nucleation in a crystal. *Nature*, 411(6838):656–656, 2001.

[5] M. A. Meyers, H. Jarmakani, E. M. Bringa, and B. A. Remington. Dislocations in shock compression and release. In J. P. Hirth and L. P. Kubin, editors, *Dislocations in Solids*, volume 15, chapter 89, pages 94–197. North-Holland, 2009.

[6] M. A. Tschopp and D. L. McDowell. Influence of single crystal orientation on homogeneous dislocation nucleation under uniaxial loading. *J. Mech. Phys. Solids*, 56:1806–1830, 2008.

[7] B. Gurrutxaga-Lerma, D. S. Balint, D. Dini, D. E. Eakins, and A. P. Sutton. A dynamic discrete dislocation plasticity method for the simulation of plastic relaxation under shock loading. *Proc. R. Soc. A.*, 469(2156), 2013.
[8] B. Gurrutxaga-Lerma, D. S. Balint, D. Dini, D. E. Eakins, and A. P. Sutton. Attenuation of the dynamic yield point of shocked aluminum using elastodynamic simulations of dislocation dynamics. *Physical review letters*, 114(17):174301, 2015.
[9] X. Markenscoff. The transient motion of a nonuniformly moving dislocation. *J. Elasticity*, **10**(2):193–201, 1980.
[10] B. Gurrutxaga-Lerma, D. S. Balint, D. Dini, and A. P. Sutton. Elastodynamic image forces on dislocations. *Proc. Roy. Soc. A*, 471(2181):20150433, 2015.
[11] T. Mura. *Micromechanics of Defects in Solids*. Martinus Nijhoff, Dordrecht, NL, 1982.
[12] J.A. Moriarty, V. Vitek, V.V. Bulatov, and S. Yip. Atomistic simulations of dislocations and defects. *J. Comput. Aided Mater. Des.*, **9**(2):99–132, 2002.
[13] V.V. Bulatov and W. Cai. *Computer simulations of dislocations*. Oxford University Press, 2013.
[14] M.W. Finnis and J.E. Sinclair. A simple empiricaln-body potential for transition metals. *Philos. Mag. A.*, **50**(1):45–55, 1984.
[15] G.J. Ackland and R. Thetford. An improved n-body semi-empirical model for body-centred cubic transition metals. *Philos. Mag. A.*, **56**(1):15–30, 1987.
[16] Daan Frenkel and Berend Smit. *Understanding molecular simulation : from algorithms to applications*. Academic Press, San Diego London, 2nd edition, 2002. Includes bibliographical references (p. [589]-617) and index.
[17] A. Sadeghirad and A. Tabarraei. A damping boundary condition for coupled atomistic continuum simulations. *Comput. Mech.*, **52**:535–551, 2013.
[18] D.R. Lide. *Handbook of chemistry and physics*. CRC, 71 edition, 1991.
[19] R.W. Balluffi. *Introduction to elasticity theory for crystal defects*. Cambridge University Press, first edition, 2012.
[20] M.L. Jokl, V. Vitek, C.J. McMahon Jr, and P. Burgers. On the micromechanicsof brittle fracture: existing vs injected cracks. *Acta metall.*, **37**(1):87–97, 1989.
[21] H. J. Stam. The two-dimensional elastodynamic distributed surface load problem. *Geophysics*, 55(8):1047–1056, 1990.
[22] K. Huang. *Quantum Field Theory: from operators to path integrals*. Wiley-VCH, Weinheim, DE., 2nd edition, 2010.
[23] N. I. Muskhelishvili. *Singular Integral Equations*. P. Noordhoff, Groningen, NL., 1953.
[24] V. Vitek, R. C. Perrin, and D. K. Bowen. The core structure of 1/2 (111) screw dislocations in bcc crystals. *Philosophical Magazine*, 21(173):1049–1073, 1970.
[25] R. Peierls. The size of a dislocation. *Proc. Phys. Soc.*, **52**(34), 1940.
[26] Y-P. Pellegrini. Dynamic peierls-nabarro equations for elastically isotropic crystals. *Phys. Rev. B*, **81**:024101, 2010.
[27] X. Markenscoff and L. Ni. The transient motion of a dislocation with a ramp-like core. *J. Mech. Phys. Solids*, 49(7):1603–1619, 2001.
[28] J. D. Achenbach. *Wave propagation in elastic solids*. North-Holland, Amsterdam, NL, 1973.

Appendix A

The solution to the system of equations given in eqn.61 is

$$C_\phi = -\frac{\beta\Delta_x}{\lambda s^3(\alpha\beta+\lambda^2)} \tag{66}$$

and

$$C_\psi = -\frac{\Delta_x}{s^3(\alpha\beta+\lambda^2)} \tag{67}$$

Thus, the U_x displacement field is given by

$$U_x = \frac{\alpha\beta\Delta_x}{\lambda s^2(\alpha\beta+\lambda^2)}e^{-s\alpha x} + \frac{\lambda\Delta_x}{s^2(\alpha\beta+\lambda^2)}e^{-s\beta x} \tag{68}$$

Invert first the spatial variable:

$$\hat{u}_x = \frac{1}{2\pi i}\int_{-i\infty}^{i\infty}\left[\frac{\alpha\beta\Delta_x}{\lambda s^2(\alpha\beta+\lambda^2)}e^{-s\alpha x} + \frac{\lambda\Delta_x}{s^2(\alpha\beta+\lambda^2)}e^{-s\beta x}\right]e^{s\lambda y}s\mathrm{d}\lambda \tag{69}$$

Two terms, one for each of the addends in the integrand, can be distinguished: a longitudinal contribution (depending on α and a), and a transverse contribution (depending on β and b).

Consider the longitudinal term first, for it is the most mathematically challenging:

$$\hat{u}_{x_a} = \frac{1}{2\pi i}\int_{-i\infty}^{i\infty}\frac{\alpha\beta\Delta_x}{\lambda s(\alpha\beta+\lambda^2)}e^{-s(\alpha x-\lambda y)}\mathrm{d}\lambda \tag{70}$$

As was done in section 4, this integral can be inverted by distorting the integration path along the imaginary axis to the Cagniard path given by

$$\tau = \alpha x - \lambda y \tag{71}$$

whereby

$$\lambda_{\pm} = \frac{-\tau y \pm i x \sqrt{t^2 - a^2 r^2}}{r^2} \tag{72}$$

The inversion can then be performed via Cagniard-de Hoop. The distorted path entails a hyperbola along the λ-plane, which can be closed at infinity with the imaginary axis. However, as in section 4, it is clear that the integrand has poles that require further considerations.

Specifically, the integrand has simple poles for

1. $\lambda = 0$
2. $\alpha\beta + \lambda^2 = 0$, which renders

$$\lambda = \pm \frac{ab}{\sqrt{a^2 + b^2}}$$

The simple pole at $\lambda = 0$ can be dealt with using the same considerations used in section 4: it will be displaced by a $-\epsilon$ quantity, and treated as a residue in the $\epsilon \to 0$ limit.

The second simple pole cannot generally be avoided, but its contribution can be computed invoking the theorem of the residues, and it is only relevant for $\tau > ab/\sqrt{a^2 + b^2} r$.

Thus, for the $x > 0$ branch:

$$\oint_{\Gamma} = -\int_{\text{Cagniard}} + \int_{R\to\infty} + \text{P}\int_{-i\infty}^{i\infty} = 2\pi i \cdot \left[\lim_{\epsilon\to 0} \text{Res}\left[\lambda = -\epsilon\right] + \text{Res}\left[\lambda = \frac{-ab}{\sqrt{a^2 + b^2}}\right]\right] \tag{73}$$

The contribution of the pole at $\lambda = 0$ can then be found as follows

$$2\pi i \lim_{\epsilon\to 0} \text{Res}\left[\lambda = -\epsilon\right] = 2\pi i \frac{\Delta_x}{s} \lim_{\epsilon\to 0}\left[\lim_{\lambda\to -\epsilon} (\lambda + \epsilon)\frac{\alpha\beta}{(\lambda + \epsilon)(\alpha\beta + \lambda^2)} e^{-s(\alpha x - \lambda y)}\right] = 2\pi i \frac{\Delta_x}{s} e^{-sax} \tag{74}$$

The second residue is found to vanish:

$$\text{Res}\left[\lambda = \frac{ab}{\sqrt{a^2 + b^2}}\right] = \lim_{\lambda\to \frac{ab}{\sqrt{a^2+b^2}}}\left[\frac{\alpha\beta\Delta_x}{\lambda s(\alpha\beta + \lambda^2)} e^{-s(\alpha x - \lambda t)} \cdot \left(\lambda - \frac{ab}{\sqrt{a^2 + b^2}}\right)\right] = 0 \tag{75}$$

The inversion of the contribution due to the Cagniard path distortion follows the usual rules of the Cagniard-de Hoop method:

$$\hat{u_x}_{\text{Cagniard}} = \frac{1}{2\pi i}\int_{ra}^{\infty} \text{Im}\left[\frac{\alpha\beta\Delta_x}{\lambda s(\alpha\beta + \lambda^2)}\frac{\partial\lambda_+}{\partial\tau}\right]_a e^{-s\tau} \text{d}\tau \tag{76}$$

whereby, by inspection, the inversion in time renders

$$u_{x_{\text{Cagniard}}} = \int_0^t \text{Im}\left[\frac{\alpha\beta\Delta_x}{\lambda(\alpha\beta + \lambda^2)}\frac{\partial\lambda_+}{\partial\tau}\right]_a \text{H}(\tau - ra)\text{H}(t - \tau)\text{d}\tau \tag{77}$$

The contribution due to the pole at $\lambda = 0$ does not required such sophisticated analysis. By properties of the Laplace transform, it is immediate that

$$u_{x_{\lambda=0}} = \text{sign}(y)\Delta_x \text{H}(t - ax) \tag{78}$$

where $\text{sign}(x)$ accounts for the reversal in the value of the residue for values of $y < 0$. This produces the desired emission along the cut surface; the Cagniard term accounts for local effects produced at the core of the dislocation ($x = 0, t = 0$), which radiate outwards.

The transverse term in β has no pole at $\lambda = 0$; thus, it will not contribute to the emission along the surface or, to put it otherwise, the emission along the cut surface lacks a transverse wave term, but still has a pole at $\lambda \pm \frac{ab}{\sqrt{a^2+b^2}}$. Equally however, the residue of this pole vanishes. Thus, its inversion can be performed along the $\tau = \beta x - \lambda t$ path, which immediately renders

$$u_{x_b} = \int_0^t \text{Im}\left[\frac{\lambda\Delta_x}{\alpha\beta + \lambda^2}\frac{\partial\lambda_+}{\partial\tau}\right]_b \text{H}(\tau - rb)\text{H}(t - \tau)\text{d}\tau \tag{79}$$

The same procedure, and analogous analysis, may be followed for solving the u_y boundary value problem.

Appendix B

The injection of an edge dislocation can also be modelled employing a similar approach to that of the screw dislocations: a $\mathbf{B} = \frac{1}{2}[111]$ edge dislocation was modelled in a tungsten cylindrical crystal, with the cylinder axis along $[10\bar{1}]$. To inject a $\mathbf{B} = \frac{1}{2}[111]$ edge dislocation, three (111) half-planes *instantaneously* are removed. The cut is therefore a void of width $\frac{\sqrt{3}d}{2}$ along $[1\bar{2}1]$ from the axis to the surface of the cylinder. During the subsequent MD relaxation the void closes through the mutual attraction of its faces, and the field of an edge dislocation in an otherwise perfect cylindrical BCC crystal is created. The displacement and stress fields converge qualitatively at long times to the continuum results. In fig.13 it can be seen that the stress and displacement fields spread from the cut. The remaining part of the paper will focus on the continuum description of the injection of a screw dislocation; the equivalent formulation for the injection of an edge dislocation will be treated in a separate contribution.

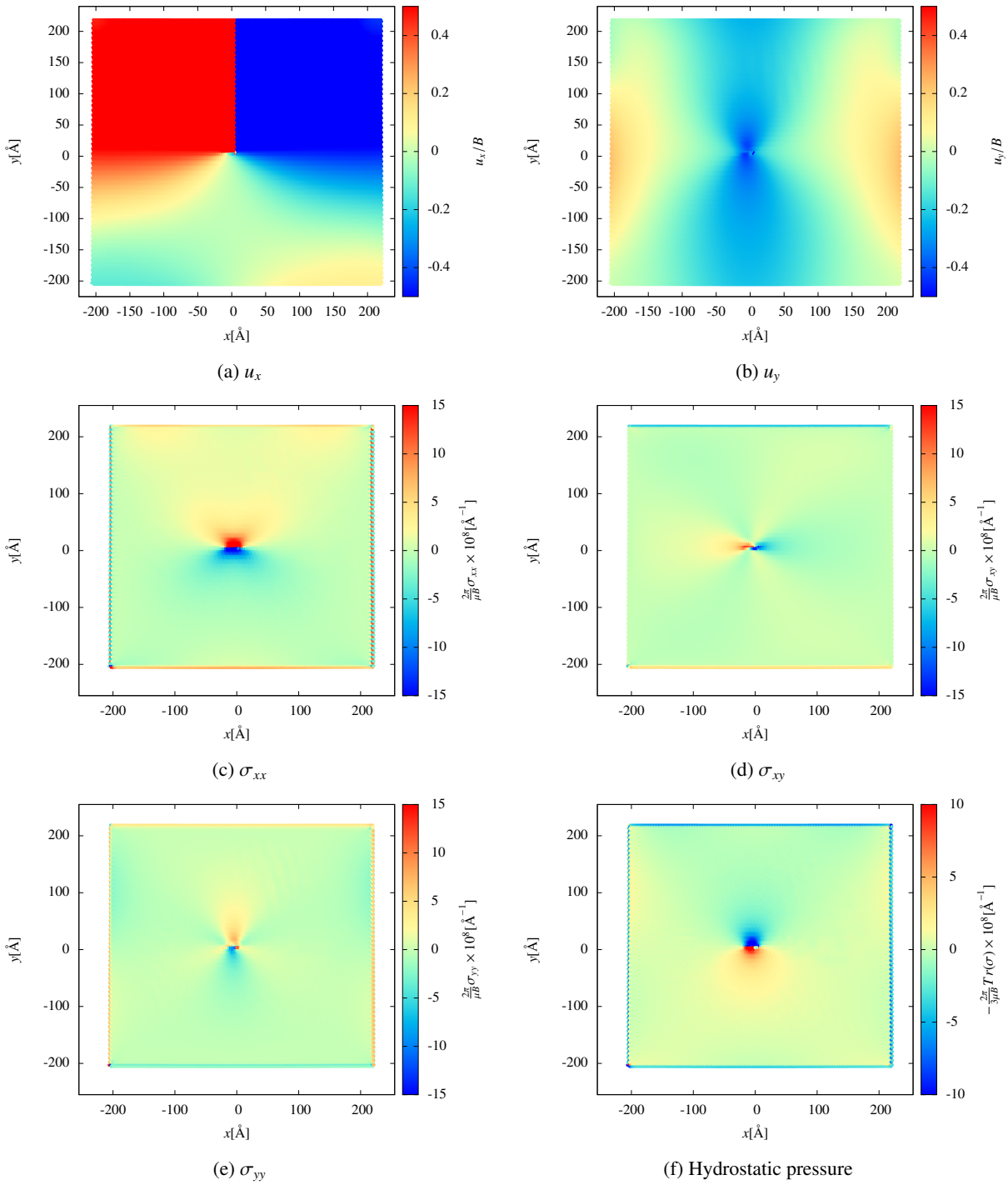

(a) u_x (b) u_y

(c) σ_{xx} (d) σ_{xy}

(e) σ_{yy} (f) Hydrostatic pressure

Figure 12: Stress and displacement fields calculated by MD 140ps after the injection of an edge dislocation.

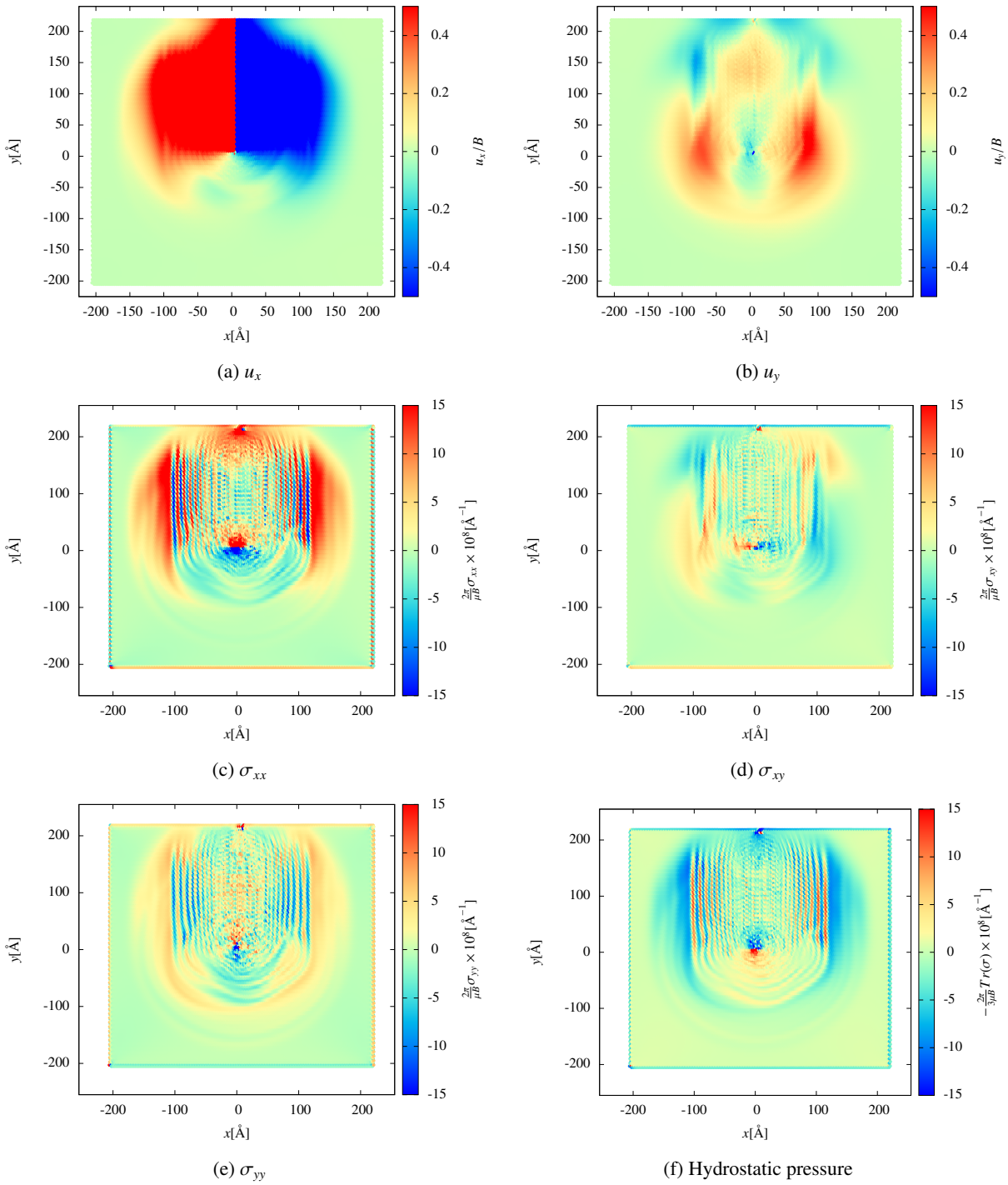

(a) u_x (b) u_y

(c) σ_{xx} (d) σ_{xy}

(e) σ_{yy} (f) Hydrostatic pressure

Figure 13: Stress and displacement fields calculated by MD 3.5ps after the injection of an edge dislocation.